

Advanced Forward Modeling and Inversion of Stokes Profiles Resulting from the Joint Action of the Hanle and Zeeman Effects

A. Asensio Ramos, J. Trujillo Bueno¹

Instituto de Astrofísica de Canarias, Vía Láctea s/n, E-38205 La Laguna, Tenerife, Spain

and

E. Landi Degl'Innocenti

*Università degli Studi di Firenze, Dipartimento di Astronomia e Scienza dello Spazio,
Largo Enrico Fermi 2, I-50125 Florence, Italy*

aasensio@iac.es, jtb@iac.es, landie@arcetri.astro.it

ABSTRACT

A big challenge in solar and stellar physics in the coming years will be to decipher the magnetism of the solar outer atmosphere (chromosphere and corona) along with its dynamic coupling with the magnetic fields of the underlying photosphere. To this end, it is important to develop rigorous diagnostic tools for the physical interpretation of spectropolarimetric observations in suitably chosen spectral lines. Here we present a computer program for the synthesis and inversion of Stokes profiles caused by the joint action of atomic level polarization and the Hanle and Zeeman effects in some spectral lines of diagnostic interest, such as those of the He I 10830 Å and 5876 Å (or D₃) multiplets. It is based on the quantum theory of spectral line polarization, which takes into account in a rigorous way all the relevant physical mechanisms and ingredients (optical pumping, atomic level polarization, level crossings and repulsions, Zeeman, Paschen-Back and Hanle effects). The influence of radiative transfer on the emergent spectral line radiation is taken into account through a suitable slab model. The user can either calculate the emergent intensity and polarization for any given magnetic field vector or infer the dynamical and magnetic properties from the observed Stokes profiles via an efficient inversion algorithm based on global optimization methods. The reliability of the forward modeling and inversion code presented

¹Consejo Superior de Investigaciones Científicas (Spain)

here is demonstrated through several applications, which range from the inference of the magnetic field vector in solar active regions to determining whether or not it is canopy-like in quiet chromospheric regions. This user-friendly diagnostic tool called “HAZEL” (from HAnle and ZEeman Light) is offered to the astrophysical community, with the hope that it will facilitate new advances in solar and stellar physics.

Subject headings: magnetic fields — polarization — radiative transfer — scattering — Sun: chromosphere — methods: data analysis, numerical

1. Introduction

The present paper describes a computer program for the synthesis and inversion of Stokes profiles resulting from the joint action of the Hanle and Zeeman effects in some spectral lines of diagnostic interest, such as those pertaining to the He I 10830 Å and 5876 Å (or D₃) multiplets. The effects of radiative transfer on the emergent spectral line radiation are taken into account through a suitable slab model. Our aim is to provide the solar and stellar physics communities with a robust but user-friendly tool for understanding and interpreting spectropolarimetric observations, with the hope that this will facilitate new advances in solar and stellar physics.

In particular, the lines of neutral helium at 10830 Å are of great interest for empirical investigations of the dynamic and magnetic properties of plasma structures in the solar chromosphere and corona, such as active regions (e.g., Harvey & Hall 1971; Rüedi et al. 1996; Lagg et al. 2004; Centeno et al. 2006), filaments (e.g., Lin et al. 1998; Trujillo Bueno et al. 2002b), prominences (e.g., Merenda et al. 2006) and spicules (e.g., Trujillo Bueno et al. 2005; Socas-Navarro & Elmore 2005). The same applies to the lines of the He I D₃ multiplet at 5876 Å which have been used for investigating the magnetic field vector in solar prominences and spicules (e.g., Landi Degl’Innocenti 1982; Querfeld et al. 1985; Bommier et al. 1994; Casini et al. 2003; López Ariste & Casini 2005; Ramelli et al. 2006a,b)

Such helium lines result from transitions between terms of the triplet system of helium (ortho-helium), whose respective J -levels (with J the level’s total angular momentum) are far less populated than the ground level of helium (that is, than the singlet level 1S_0), except perhaps in flaring regions. On the other hand, the lower term ($2s^3S_1$) of the He I 10830 Å multiplet is the ground level of ortho-helium, while its upper term ($2p^3P_{2,1,0}$) is the lower one of 5876 Å (whose upper term is $3d^3D_{3,2,1}$). Therefore, the significant difference in the ensuing optical thicknesses of the observed solar plasma structure implies that when the radiation

in these spectral lines is observed on the solar disk it is much easier to see structures in 10830 Å than in 5876 Å, while both lines are clearly seen in emission when observing off-limb structures such as prominences and spicules. The additional fact that the Hanle effect in forward scattering creates measurable linear polarization signals in the lines of the He I 10830 Å multiplet when the magnetic field is inclined with respect to the local solar vertical direction (Trujillo Bueno et al. 2002b), and that there is a nearby photospheric line of Si I, makes the 10830 Å spectral region very suitable for investigating the coupling between the photosphere and the corona.

While the Stokes I profiles of the 10830 Å and 5876 Å helium lines depend mainly on the distribution of the populations of their respective upper (J_u) and lower (J_l) levels along the line-of-sight (LOS), their Stokes Q , U and V profiles depend on the strengths and wavelength positions of the π ($\Delta M = M_u - M_l = 0$), σ_{blue} ($\Delta M = +1$) and σ_{red} ($\Delta M = -1$) transitions, which can only be calculated correctly within the framework of the Paschen-Back effect theory. Moreover, the Q , U and V profiles are also affected by the atomic level polarization induced by anisotropic pumping processes (e.g., Landi Degl’Innocenti & Landolfi 2004). An atomic level of total angular momentum J is said to be polarized when its magnetic sublevels are unequally populated and/or when there are quantum coherences between them. The radiative transitions induced by the anisotropic illumination of the helium atoms in the solar atmosphere are able to create a significant amount of atomic polarization in the helium levels, even in the metastable lower level of the He I 10830 Å multiplet (Trujillo Bueno et al. 2002b). If the net circular polarization of the incident radiation at the wavelengths of the helium transitions is negligible, as it uses to be the case, the radiatively induced atomic level polarization is such that the populations of substates with different values of $|M|$ are different (non-zero atomic alignment), while substates with magnetic quantum numbers M and $-M$ are equally populated (zero atomic orientation). On the other hand, elastic collisions with the neutral hydrogen atoms of the solar chromospheric and coronal structures are unable to destroy the atomic polarization of the He I levels. As a result, even in the absence of magnetic fields, linearly polarized spectral line radiation would be produced, simply because the population imbalances among the magnetic sublevels imply more or fewer π -transitions, per unit volume and time, than σ transitions. The atomic polarization of the upper level of the line transition under consideration is thus responsible of a *selective emission* of polarization components, while that of the lower level may give rise to a *selective absorption* of polarization components (“zero-field” dichroism). In order for this type of dichroism to produce a measurable contribution to the emergent linear polarization it is necessary to have a substantial line-center optical thickness along the LOS or, assuming a small but non-negligible optical thickness, that the plasma structure under consideration is observed against the bright background of the solar disk (Trujillo Bueno et al. 2002b;

Trujillo Bueno & Asensio Ramos 2007). Therefore, the observable effects of dichroism are easier to detect in He I 10830 Å than in 5876 Å.

In the presence of a magnetic field the emergent polarization changes because of the following two reasons. First, because a magnetic field modifies the atomic level polarization, not only by producing the Hanle-effect relaxation of the quantum coherences pertaining to each individual J -level, but also through possible interferences between the magnetic sub-levels pertaining to different J -levels, which give rise to a variety of remarkable effects such as the transfer of atomic alignment to atomic orientation in the J -levels of the upper term of the He I D₃ multiplet (Landi Degl’Innocenti 1982) or the enhancement of the scattering polarization in the D₂ line of Na I by a vertical magnetic field (Trujillo Bueno et al. 2002a). Second, because the magnetic splitting of the atomic energy levels give rise to significant wavelength shifts between the π and σ transitions (as compared with the spectral line width) and, consequently, to the generation of measurable linear and/or circular polarization (i.e., the familiar transverse and longitudinal Zeeman effects, respectively). Obviously, a correct modeling of the spectral line polarization that results from the joint action of the Hanle and Zeeman effects requires the application of the quantum theory of spectral line polarization (see the monograph by Landi Degl’Innocenti & Landolfi 2004), as done by several researchers for interpreting spectropolarimetric observations of solar plasma structures in the He I D₃ multiplet (e.g., Landi Degl’Innocenti 1982; Bommier et al. 1994; Casini et al. 2003; López Ariste & Casini 2005) and in the He I 10830 Å triplet (e.g., Trujillo Bueno et al. 2002b, 2005; Merenda et al. 2006).

Over the last few years new computer programs for the synthesis and inversion of Stokes profiles induced by the joint action of atomic level polarization and the Hanle and Zeeman effects have been developed and applied to the interpretation of spectropolarimetric observations. For example, Landi Degl’Innocenti & Landolfi (2004) have developed some forward modeling codes with which they have calculated several Hanle effect diagrams and theoretical Stokes profiles of lines from complex atomic models, while the computer program of Casini & Manso Sainz (2005) can treat even the case of a hyperfine structured multiplet taking into account the quantum interferences between the F levels belonging to the J levels of different terms. Concerning Stokes inversion techniques we should mention that Casini et al. (2003) applied an inversion code based on principal component analysis (López Ariste & Casini 2002) to spectropolarimetric observations of solar prominences in the He I D₃ multiplet, providing two-dimensional maps of the magnetic field vector and further evidence for strengths significantly larger than average. On the other hand, Merenda et al. (2006) opted for an inversion strategy for the He I 10830 Å multiplet in which the longitudinal component of the magnetic field vector is obtained from the measured Stokes V profiles (which are dominated by the Zeeman effect for the lines of the He I 10830 Å multiplet), and

its orientation from the observed Stokes Q and U profiles (which in solar prominences are due to the presence of atomic level polarization). In the just mentioned computer programs and applications the optically thin assumption was used, which was a suitable approximation for the particular prominences observed, but an unreliable one in general (and especially for the interpretation of observations in the He I 10830 Å multiplet).

A simple but suitable model for taking into account radiative transfer effects is the constant-property slab model used by Trujillo Bueno et al. (2002b, 2005) for the interpretation of spectropolarimetric observations in solar filaments and spicules, which has been recently extended by Trujillo Bueno & Asensio Ramos (2007) to include magneto-optical effects. These authors have applied this “cloud” model for the interpretation of spectropolarimetric observations in order to point out that the atomic polarization of the helium levels may have an important impact on the emergent linear polarization of the He I 10830 Å multiplet, even for magnetic field strengths as large as 1000 G. Therefore, inversion codes that neglect the influence of atomic level polarization, such as the Milne-Eddington codes of Lagg et al. (2004) and Socas-Navarro et al. (2004), should ideally be used only for the inversion of Stokes profiles emerging from strongly magnetized regions (with $B > 1000$ G), or when the observed Stokes Q and U profiles turn out to be dominated by the transverse Zeeman effect (e.g., as it happens with some active regions filaments as a result of the particular illumination conditions explained in Trujillo Bueno & Asensio Ramos 2007).

It is also necessary to mention that Manso Sainz & Trujillo Bueno (2003a) developed a general radiative transfer computer program for solving the so-called non-LTE problem of the 2nd kind –that is, the multilevel scattering polarization problem including the Hanle effect of a weak magnetic field. These authors considered the multilevel atom approximation (which neglects quantum interferences between the sublevels of *different* J -levels), but took fully into account the effects of radiative transfer in realistic atmospheric models and the role of elastic and inelastic collisions in addition to all the relevant optical pumping mechanisms. An interesting application using a semi-empirical model of the solar atmosphere can be found in Manso Sainz & Trujillo Bueno (2003b). The recent advances in the development of efficient numerical methods for the solution of non-LTE polarization transfer problems (e.g., the review by Trujillo Bueno 2003) and in computer technology make now possible even the performing of three-dimensional radiative transfer simulations of the Hanle effect in convective atmospheres (e.g., Trujillo Bueno & Shchukina 2007).

The previous introductory paragraphs strongly suggest that it would be of great interest to develop a robust but user-friendly computer program for the synthesis and inversion of Stokes profiles resulting from the joint action of atomic level polarization and the Hanle and Zeeman effects. We have done this by implementing an efficient global optimization

method for the solution of the inversion problem and by calculating at each iterative step the emergent spectral line polarization through the solution of the Stokes-vector transfer equation in a slab of constant physical properties in which the radiatively-induced atomic level polarization is assumed to be dominated by the photospheric continuum radiation. At each point of the observed field of view the slab’s optical thickness is chosen to fit the Stokes I profile, which is a strategy that accounts implicitly for the true physical mechanisms that populate the triplet levels of He I (e.g., the photoionization-recombination mechanism, as shown by Centeno et al. 2008). The observed Stokes Q , U and V profiles are then used to infer the magnetic field vector along with a few extra physical quantities.

The outline of this paper is as follows. The formulation of the problem is presented in §2, where we review the relevant equations within the framework of the quantum theory of spectral line polarization. The forward modelling option of our computer program is described in §3, including some interesting examples of possible applications. §4 deals with a detailed description of the Stokes inversion option, while §5 considers a variety of applications aimed at an in-depth testing of this diagnostic tool. The important issue of the possible ambiguities and degeneracies is addressed in §6, with emphasis on the Van Vleck ambiguity and on the possibility of inferring the atmospheric height at which the observed on-disk plasma structure is located. Finally, in §7 we summarize the main conclusions and comment on some ongoing developments.

2. Formulation of the problem

We consider a constant-property slab of He I atoms, located at a height h above the visible solar “surface”, in the presence of a deterministic magnetic field of arbitrary strength B , inclination θ_B and azimuth χ_B (see Fig. 1). The slab’s optical thickness at the wavelength and line of sight under consideration is τ . We assume that all the He I atoms inside this slab are illuminated from below by the photospheric solar continuum radiation field, whose center-to-limb variation has been tabulated by Pierce (2000). The ensuing anisotropic radiation pumping produces population imbalances and quantum coherences between pairs of magnetic sublevels, even among those pertaining to the different J -levels of the adopted He I atomic model. This atomic level polarization and the Zeeman-induced wavelength shifts between the π ($\Delta M = M_u - M_l = 0$), σ_{blue} ($\Delta M = +1$) and σ_{red} ($\Delta M = -1$) transitions produce polarization in the emergent spectral line radiation.

In order to facilitate the reading and understanding of this paper, in the following subsections we summarize the basic equations which allow us to calculate the spectral line polarization taking rigorously into account the joint action of the Hanle and Zeeman effects.

To this end, we have applied the quantum theory of spectral line polarization, which is described in great detail in the monograph by Landi Degl’Innocenti & Landolfi (2004). We have also applied several methods of solution of the Stokes-vector transfer equation, some of which can be considered as particular cases of the two general methods explained in §6 of Trujillo Bueno (2003).

2.1. The radiative transfer approach

The emergent Stokes vector $\mathbf{I}(\nu, \boldsymbol{\Omega}) = (I, Q, U, V)^\dagger$ (with \dagger =transpose, ν the frequency and $\boldsymbol{\Omega}$ the unit vector indicating the direction of propagation of the ray) is obtained by solving the radiative transfer equation

$$\frac{d}{ds}\mathbf{I}(\nu, \boldsymbol{\Omega}) = \boldsymbol{\epsilon}(\nu, \boldsymbol{\Omega}) - \mathbf{K}(\nu, \boldsymbol{\Omega})\mathbf{I}(\nu, \boldsymbol{\Omega}), \quad (1)$$

where s is the geometrical distance along the ray under consideration, $\boldsymbol{\epsilon}(\nu, \boldsymbol{\Omega}) = (\epsilon_I, \epsilon_Q, \epsilon_U, \epsilon_V)^\dagger$ is the emission vector and

$$\mathbf{K} = \begin{pmatrix} \eta_I & \eta_Q & \eta_U & \eta_V \\ \eta_Q & \eta_I & \rho_V & -\rho_U \\ \eta_U & -\rho_V & \eta_I & \rho_Q \\ \eta_V & \rho_U & -\rho_Q & \eta_I \end{pmatrix} \quad (2)$$

is the propagation matrix. Alternatively, introducing the optical distance along the ray, $d\tau = -\eta_I ds$, one can write the Stokes-vector transfer Eq. (1) in the following two ways:

- The first one, whose formal solution requires the use of the evolution operator introduced by Landi Degl’Innocenti & Landi Degl’Innocenti (1985), is

$$\frac{d}{d\tau}\mathbf{I} = \mathbf{K}^*\mathbf{I} - \mathbf{S}, \quad (3)$$

where $\mathbf{K}^* = \mathbf{K}/\eta_I$ and $\mathbf{S} = \boldsymbol{\epsilon}/\eta_I$. The formal solution of this equation can be seen in eq. (23) of Trujillo Bueno (2003).

- The second one, whose formal solution does not require the use of the above-mentioned evolution operator is (e.g., Rees et al. 1989)

$$\frac{d}{d\tau}\mathbf{I} = \mathbf{I} - \mathbf{S}_{\text{eff}}, \quad (4)$$

where the effective source-function vector $\mathbf{S}_{\text{eff}} = \mathbf{S} - \mathbf{K}'\mathbf{I}$, being $\mathbf{K}' = \mathbf{K}^* - \mathbf{1}$ (with $\mathbf{1}$ the unit matrix). The formal solution of this equation can be seen in eq. (26) of Trujillo Bueno (2003).

Once the coefficients ϵ_I and ϵ_X (with $X = Q, U, V$) of the emission vector and the coefficients η_I, η_X , and ρ_X of the 4×4 propagation matrix are known at each point within the medium it is possible to solve formally Eq. (3) or Eq. (4) for obtaining the emergent Stokes profiles for any desired line of sight. Our computer program considers the following levels of sophistication for the solution of the radiative transfer equation:

- *Numerical Solutions.* The most general case, where the properties of the slab vary along the ray path, has to be solved numerically. To this end, two efficient and accurate methods of solution of the Stokes-vector transfer equation are those proposed by Trujillo Bueno (2003) (see his eqs. (24) and (27), respectively). The starting points for the development of these two numerical methods were Eq. (3) and Eq. (4), respectively. Both methods can be considered as generalizations, to the Stokes-vector transfer case, of the well-known short characteristics method for the solution of the standard (scalar) transfer equation.
- *Exact analytical solution of the problem of a constant-property slab including the magneto-optical terms of the propagation matrix.* For the general case of a constant-property slab of arbitrary optical thickness we actually have the following analytical solution, which can be easily obtained as a particular case of eq. (24) of Trujillo Bueno (2003):

$$\mathbf{I} = e^{-\mathbf{K}^*\tau} \mathbf{I}_{\text{sun}} + [\mathbf{K}^*]^{-1} (\mathbf{1} - e^{-\mathbf{K}^*\tau}) \mathbf{S}, \quad (5)$$

where \mathbf{I}_{sun} is the Stokes vector that illuminates the slab's boundary that is most distant from the observer. We point out that the exponential of the propagation matrix \mathbf{K}^* has an analytical expression similar to eq. (8.23) in Landi Degl'Innocenti & Landolfi (2004).

- *Approximate analytical solution of the problem of a constant-property slab including the magneto-optical terms of the propagation matrix.* An approximate analytical solution to the constant-property slab problem can be easily obtained as a particular case of eq. (27) of Trujillo Bueno (2003):

$$\mathbf{I} = [\mathbf{1} + \Psi_0 \mathbf{K}']^{-1} [(e^{-\tau} \mathbf{1} - \Psi_M \mathbf{K}') \mathbf{I}_{\text{sun}} + (\Psi_M + \Psi_0) \mathbf{S}], \quad (6)$$

where the coefficients Ψ_M and Ψ_0 depend only on the optical thickness of the slab at the frequency and line-of-sight under consideration, since their expressions are:

$$\begin{aligned}\Psi_M &= \frac{1 - e^{-\tau}}{\tau} - e^{-\tau}, \\ \Psi_0 &= 1 - \frac{1 - e^{-\tau}}{\tau}.\end{aligned}\tag{7}$$

Note that Eq. (6) for the emergent Stokes vector is the one used by Trujillo Bueno & Asensio Ramos (2007) for investigating the impact of atomic level polarization on the Stokes profiles of the He I 10830 Å multiplet. We point out that, strictly speaking, it can be considered only as the exact analytical solution of the optically-thin constant-property slab problem¹. The reason why Eq. (6) is, in general, an approximate expression for calculating the emergent Stokes vector is because its derivation assumes that the Stokes vector within the slab varies linearly with the optical distance. However, it provides a fairly good approximation to the emergent Stokes profiles (at least for all the problems we have investigated in this paper). Moreover, the results of fig. 2 of Trujillo Bueno & Asensio Ramos (2007) remain also virtually the same when using instead the exact Eq. (5), which from a computational viewpoint is significantly less efficient than the approximate Eq. (6).

- *Exact analytical solution of the problem of a constant-property slab when neglecting the second-order terms of the Stokes-vector transfer equation.* Simplified expressions for the emergent Stokes vector can be obtained when $\epsilon_I \gg \epsilon_X$ and $\eta_I \gg (\eta_X, \rho_X)$, which justifies to neglect the second-order terms of Eq. (1). The resulting approximate formulae for the emergent Stokes parameters are given by eqs. (9) and (10) of Trujillo Bueno & Asensio Ramos (2007), which are identical to those used by Trujillo Bueno et al. (2005) for modeling the Stokes profiles observed in solar chromospheric spicules. We point out that there is a typing error in the sentence that introduces such eqs. (9) and (10) in Trujillo Bueno & Asensio Ramos (2007), since they are obtained only when the above-mentioned second-order terms are neglected in Eq. (1), although it is true that there are no magneto-optical terms in the resulting equations.
- *Optically thin limit.* Finally, the most simple solution is obtained when taking the optically thin limit ($\tau \ll 1$) in the equations reported in the previous point, which lead to the equations (11) and (12) of Trujillo Bueno & Asensio Ramos (2007). Note that if $\mathbf{I}_{\text{sun}} = 0$ (i.e., $I_0 = X_0 = 0$), then such optically thin equations imply that $X/I \approx \epsilon_X/\epsilon_I$.

¹More precisely, when the optical thickness of the slab is small in comparison with the eigenvalues of the matrix \mathbf{K}' .

The coefficients of the emission vector and of the propagation matrix depend on the multipolar components, $\rho_Q^K(J, J')$, of the atomic density matrix. Let us recall now the meaning of these physical quantities and how to calculate them in the presence of an arbitrary magnetic field under given illumination conditions.

2.2. The multipolar components of the atomic density matrix

We quantify the atomic polarization of the He I levels using the multipolar components of the atomic density matrix. The He I atom can be correctly described under the framework of the L - S coupling (e.g., Condon & Shortley 1935). As illustrated in Fig. 2, the different J -levels are grouped in terms with well defined values of the electronic angular momentum L and the spin S . Since the ^4He atoms are devoid of nuclear angular momentum, we do not have to consider hyperfine structure². The energy separation between the J -levels pertaining to each term is very small in comparison with the energy difference between different terms. For example, the energy separation between the $J = 3$ and $J = 2$ levels of the term $3d^3D$ (the upper term of the D_3 multiplet) is of the order of 0.0025 cm^{-1} , which is $\sim 2 \times 10^5$ times smaller than the separation between the $3d^3D$ and $3p^3P$ terms. On the other hand, although the energy separations between the J -levels of the upper terms of the 10830 Å and D_3 multiplets are much larger than their natural widths, such J -levels suffer crossings and repulsions for the typical magnetic strengths encountered in the solar atmospheric plasma (e.g., the $J = 2$ and $J = 1$ levels of the upper term of the He I 10830 Å multiplet cross for magnetic strengths between 400 G and 1600 G, while the $J = 3$ and $J = 2$ levels of the upper term of the D_3 multiplet cross for strengths between 10 G and 100 G, approximately). This can be seen clearly in Fig. 3. Therefore, it turns out to be fundamental to allow for coherences between different J -levels pertaining to the same term but not between the J -levels pertaining to different terms. As a result, we can represent the atom under the formalism of the multi-term atom discussed by Landi Degl’Innocenti & Landolfi (2004).

In the absence of magnetic fields the energy eigenvectors can be written using Dirac’s notation as $|\beta LSJM\rangle$, where β indicates a set of inner quantum numbers specifying the electronic configuration. In general, if a magnetic field of arbitrary strength is present, the vectors $|\beta LSJM\rangle$ are no longer eigenfunctions of the total Hamiltonian and J is no longer a good quantum number. In this case, the eigenfunctions of the full Hamiltonian can be

²See Belluzzi, Trujillo Bueno, & Landi Degl’Innocenti (2007) for the formulation and solution of an interesting problem where hyperfine structure is important.

written as the following linear combination:

$$|\beta LS j M\rangle = \sum_J C_J^j(\beta LS, M) |\beta LS J M\rangle, \quad (8)$$

where j is a pseudo-quantum number which is used for labeling the energy eigenstates belonging to the subspace corresponding to assigned values of the quantum numbers β , L , S , and M , and where the coefficients C_J^j can be chosen to be real.

In the presence of a magnetic field sufficiently weak so that the magnetic energy is much smaller than the energy intervals between the J -levels, the energy eigenvectors are still of the form $|\beta LS J M\rangle$ ($C_J^j(\beta LS, M) \approx \delta_{Jj}$), and the splitting of the magnetic sublevels pertaining to each J -level is linear with the magnetic field strength. For stronger magnetic fields, we enter the incomplete Paschen-Back effect regime in which the energy eigenvectors are of the general form given by Eq. (8), and the splitting among the various M -sublevels is no longer linear with the magnetic strength. This regime is reached for magnetic strengths of the order of 10 G for the He I D_3 multiplet and of the order of 100 G for the 10830 Å multiplet (see Fig. 3). If the magnetic field strength is further increased we eventually reach the so-called complete Paschen-Back effect regime, where the energy eigenvectors are of the form $|LSM_L M_S\rangle$ and each L - S term splits into a number of components, each of which corresponding to particular values of $(M_L + 2M_S)$.

Within the framework of the multi-term atom model the atomic polarization of the energy levels is described with the aid of the density matrix elements

$$\rho^{\beta LS}(jM, j'M') = \langle \beta LS j M | \rho | \beta LS j' M' \rangle, \quad (9)$$

where ρ is the atomic density matrix operator. Using the expression of the eigenfunctions of the total Hamiltonian given by Eq. (8), the density matrix elements can be rewritten as:

$$\rho^{\beta LS}(jM, j'M') = \sum_{JJ'} C_J^j(\beta LS, M) C_{J'}^{j'}(\beta LS, M') \rho^{\beta LS}(JM, J'M'), \quad (10)$$

where $\rho^{\beta LS}(JM, J'M')$ are the density matrix elements on the basis of the eigenvectors $|\beta LS J M\rangle$.

Following Landi Degl'Innocenti & Landolfi (2004), it is helpful to use the spherical statistical tensor representation, which is related to the previous one by the following linear combination:

$$\begin{aligned} {}^{\beta LS} \rho_Q^K(J, J') &= \sum_{jj'MM'} C_J^j(\beta LS, M) C_{J'}^{j'}(\beta LS, M') \\ &\times (-1)^{J-M} \sqrt{2K+1} \begin{pmatrix} J & J' & K \\ M & -M' & -Q \end{pmatrix} \rho^{\beta LS}(jM, j'M'), \end{aligned} \quad (11)$$

where the 3-j symbol is defined as indicated by any suitable textbook on Racah algebra. This alternative representation has some advantages. Firstly, the well-known results obtained when atomic polarization effects are disregarded are easily recovered by considering only the elements of the density matrix with $K = 0$ and $Q = 0$. Secondly, the transformation law under rotations is much simpler because it involves only one rotation matrix. Finally, each ρ_Q^K element has a clear physical interpretation: the ρ_Q^2 elements (with $Q = 0, \pm 1, \pm 2$) are called the atomic alignment components, while the ρ_Q^1 elements (with $Q = 0, \pm 1$) are the atomic orientation components. The ${}^{\beta LS}\rho_Q^K(J, J')$ elements are, in general, complex quantities (except for the elements with $Q = 0$ and $J = J'$, that are real quantities), so that, taking into account that the density matrix is an hermitian operator, the number of real quantities required to describe the atomic polarization properties of a given L - S term is $(2S + 1)^2(2L + 1)^2$. This makes a total of 405 real quantities to describe the atomic polarization of the 5-term model atom shown in Fig. 2.

2.3. Statistical equilibrium equations

In order to obtain the ${}^{\beta LS}\rho_Q^K(J, J')$ elements we have to solve the statistical equilibrium equations. These equations, written in a reference system in which the quantization axis (Z) is directed along the magnetic field vector and neglecting the influence of collisions, can be written as (Landi Degl'Innocenti & Landolfi 2004):

$$\begin{aligned}
 \frac{d}{dt} {}^{\beta LS}\rho_Q^K(J, J') &= -2\pi i \sum_{K'Q'} \sum_{J''J'''} N_{\beta LS}(KQJJ', K'Q'J''J''') {}^{\beta LS}\rho_{Q'}^{K'}(J'', J''') \\
 &+ \sum_{\beta_\ell L_\ell K_\ell Q_\ell J_\ell J'_\ell} \beta_\ell L_\ell S \rho_{Q_\ell}^{K_\ell}(J_\ell, J'_\ell) \mathbb{T}_A(\beta LS K Q J J', \beta_\ell L_\ell S K_\ell Q_\ell J_\ell J'_\ell) \\
 &+ \sum_{\beta_u L_u K_u Q_u J_u J'_u} \beta_u L_u S \rho_{Q_u}^{K_u}(J_u, J'_u) \left[\mathbb{T}_E(\beta LS K Q J J', \beta_u L_u S K_u Q_u J_u J'_u) \right. \\
 &\quad \left. + \mathbb{T}_S(\beta LS K Q J J', \beta_u L_u S K_u Q_u J_u J'_u) \right] \\
 &- \sum_{K'Q'J''J'''} {}^{\beta LS}\rho_{Q'}^{K'}(J'', J''') \left[\mathbb{R}_A(\beta LS K Q J J' K' Q' J'' J''') \right. \\
 &\quad \left. + \mathbb{R}_E(\beta LS K Q J J' K' Q' J'' J''') + \mathbb{R}_S(\beta LS K Q J J' K' Q' J'' J''') \right]. \quad (12)
 \end{aligned}$$

The first term in the right hand side of Eq. (12) takes into account the influence of the magnetic field on the atomic level polarization. This term has its simplest expression in the chosen magnetic field reference frame (see eq. 7.41 of Landi Degl'Innocenti & Landolfi 2004). In any other reference system, a more complicated expression arises. The second,

third and fourth terms account, respectively, for coherence transfer due to absorption from lower levels (\mathbb{T}_A), spontaneous emission from upper levels (\mathbb{T}_E) and stimulated emission from upper levels (\mathbb{T}_S). The remaining terms account for the relaxation of coherences due to absorption to upper levels (\mathbb{R}_A), spontaneous emission to lower levels (\mathbb{R}_E) and stimulated emission to lower levels (\mathbb{R}_S), respectively.

The stimulated emission and absorption transfer and relaxation rates depend explicitly on the radiation field properties (see eqs. 7.45 and 7.46 of Landi Degl’Innocenti & Landolfi 2004). The symmetry properties of the radiation field are accounted for by the spherical components of the radiation field tensor:

$$J_Q^K(\nu) = \oint \frac{d\Omega}{4\pi} \sum_{i=0}^3 \mathcal{T}_Q^K(i, \mathbf{\Omega}) S_i(\nu, \mathbf{\Omega}). \quad (13)$$

The quantities $\mathcal{T}_Q^K(i, \mathbf{\Omega})$ are spherical tensors that depend on the reference frame and on the ray direction $\mathbf{\Omega}$. They are given by

$$\mathcal{T}_Q^K(i, \mathbf{\Omega}) = \sum_P t_P^K(i) \mathcal{D}_{PQ}^K(R'), \quad (14)$$

where R' is the rotation that carries the reference system defined by the line-of-sight $\mathbf{\Omega}$ and by the polarization unit vectors \mathbf{e}_1 and \mathbf{e}_2 into the reference system of the magnetic field, while $\mathcal{D}_{PQ}^K(R')$ is the usual rotation matrix (e.g., Edmonds 1960). Table 5.6 in Landi Degl’Innocenti & Landolfi (2004) gives the $\mathcal{T}_Q^K(i, \mathbf{\Omega})$ values for each Stokes parameter S_i (with $S_0 = I$, $S_1 = Q$, $S_2 = U$ and $S_3 = V$).

2.4. Emission and absorption coefficients

Once the multipolar components ${}^{\beta LS} \rho_Q^K(J, J')$ are known, the coefficients ϵ_I and ϵ_X (with $X = Q, U, V$) of the emission vector and the coefficients η_I , η_X , and ρ_X of the propagation matrix for a given transition between an upper term ($\beta L_u S$) and a lower term ($\beta L_\ell S$) can be calculated with the expressions of §7.6.b in Landi Degl’Innocenti & Landolfi (2004). These radiative transfer coefficients are proportional to the number density of He I atoms, \mathcal{N} . Their defining expressions contain also the Voigt profile and the Faraday-Voigt profile (see §5.4 in Landi Degl’Innocenti & Landolfi 2004), which involve the following parameters: a (i.e., the reduced damping constant), v_{th} (i.e., the velocity that characterizes the thermal motions, which broaden the line profiles), and v_{mac} (i.e., the velocity of possible bulk motions in the plasma, which produce a Doppler shift).

It is important to emphasize that the expressions for the emission and absorption coefficients and those of the statistical equilibrium equations are written in the reference system whose quantization axis is parallel to the magnetic field. The following equation indicates how to obtain the density matrix elements in a new reference system:

$$[\beta^{LS} \rho_Q^K(J, J')]_{\text{new}} = \sum_{Q'} [\beta^{LS} \rho_{Q'}^K(J, J')]_{\text{old}} \mathcal{D}_{Q'Q}^K(R)^*, \quad (15)$$

where $\mathcal{D}_{Q'Q}^K(R)^*$ is the complex conjugate of the rotation matrix for the rotation R that carries the old reference system into the new one.

2.5. The atomic model

The atomic model we have used in our calculations includes the following five terms of the triplet system of neutral helium: $2s^3S$, $3s^3S$, $2p^3P$, $3s^3P$ and $3d^3D$ (see Fig. 2). It has been concluded that the inclusion of these five terms is sufficient for a reliable calculation of the atomic polarization that the anisotropic pumping of the photospheric continuum radiation produces in the lower and upper J -levels of the D_3 multiplet (Bommier 1980). Since the only level (with $J = 1$) of the lower term $2s^3S$ is metastable, the adopted atomic model should be also satisfactory for the 10830 Å multiplet. In order to check this we have compared the results obtained using two different atomic models. The first one is that of Fig. 2. The second one is a simplified version in which only the $2s^3S$, $2p^3P$ and $3d^3D$ terms are taken into account. We have verified, for a large number of possible configurations, that differences in the resulting values of the multipolar components of the atomic density matrix are never larger than $\sim 5\%$ for the terms involved in the 10830 Å transitions. Although the selection rules allow six transitions among the 5 terms, we have only included the four transitions indicated in Fig. 2 (i.e., we have neglected the influence of the infrared transitions $3d^3D$ - $3p^3P$ and $3p^3P$ - $3s^3S$). The Einstein coefficients for the four included transitions shown in Table 3 and the energy of the levels shown in Fig. 2 have been obtained from the NIST database³ (see also Wiese et al. 1966; Drake & Martin 1998). Table 3 also indicates the value of the critical magnetic field strength for the operation of the upper-level Hanle effect, which results from equating the Zeeman splitting of the level with its natural width:

$$B_{\text{critical}} \approx 1.137 \times 10^{-7} / (t_{\text{life}} g_L), \quad (16)$$

³<http://physics.nist.gov/PhysRefData/ASD/index.html>

where t_{life} is the level’s lifetime in seconds, g_L is its Landé factor and B_{critical} is given in gauss. Note that for obtaining the $B_{\text{critical}}^{\text{upper}}$ values of Table 3 we have used $t_{\text{life}} \approx 1/A_{ul}$, while an estimation of the critical magnetic field strength for the operation of the lower-level Hanle effect requires using $t_{\text{life}} \approx 1/(B_{lu}J_0^0)$ (which for the metastable lower-level of the He I 10830 Å multiplet gives $B_{\text{critical}}^{\text{lower}} \approx 0.1$ G).

We point out that in our modeling we are not explicitly taking into account the radiative mechanism that is thought to be responsible of the overpopulation of the triplet levels of He I required to produce the absorption or emission features observed in the spectral lines of such two multiplets –that is, ionizations from the singlet states of He I caused by EUV ionizing radiation coming downwards from the corona followed by recombinations towards both the singlet and triplet states (e.g., Avrett et al. 1994). The fact that most of the ionizations take place from the singlet states suggests that the atomic polarization of the triplet states should be little affected by such EUV coronal irradiation. This expectation is reinforced by the fact that the number of photoionizations per unit volume and time from the triplet levels of He I is way smaller than the number of bound-bound transitions (see Fig. 7 in Centeno et al. 2008), which suggests that the atomic polarization of the J -levels of the 10830 Å and D₃ multiplets is indeed dominated by optical pumping in the line transitions themselves. Following our approach, the key mechanism responsible of the absorption or emission observed in such lines of neutral helium, be it the above-mentioned photoionization-recombination mechanism and/or collisional excitation in regions with $T > 20000$ K (cf., Andretta & Jones 1997), is unimportant in our forward modeling and inversion approach. The reason is that they are implicitly accounted for via the definition of the optical thickness of the slab which, being a free parameter in our modeling, is used to fit the observed intensity profiles. This point has been clarified by Centeno et al. (2008).

2.6. The incident radiation field

As mentioned before, we consider a slab of He I atoms anisotropically illuminated from below by the photospheric continuum radiation, which we assume to have axial symmetry around the solar local vertical direction. Since the illumination conditions are assumed to be known a priori, the radiation field tensors can be calculated directly from the given incident radiation.

For symmetry reasons, it is advantageous to calculate the statistical tensors of the radiation field in a reference frame in which the Z -axis is along the vertical of the atmosphere. Since the incoming radiation is assumed to be unpolarized, the only non-zero spherical tensor components of the radiation field are J_0^0 and J_0^2 . They quantify the mean intensity and the

“degree of anisotropy” of the radiation field, respectively. For the case of our plane-parallel slab model, their expressions reduce to:

$$J_0^0 = \frac{1}{2} \int_{-1}^1 I(\mu) d\mu \quad (17)$$

$$J_0^2 = \frac{1}{2\sqrt{2}} \int_{-1}^1 (3\mu^2 - 1)I(\mu) d\mu, \quad (18)$$

where $\mu = \cos \theta$ is the cosine of the heliocentric angle θ .

It is convenient to parameterize the radiation field in terms of the number of photons per mode \bar{n} and the anisotropy factor w :

$$\bar{n} = \frac{c^2}{2h\nu^3} J_0^0, \quad w = \sqrt{2} \frac{J_0^2}{J_0^0}, \quad (19)$$

where c is the light speed, h is the Planck constant and ν is the frequency of the transition. The anisotropy factor fulfills $-1/2 \leq w \leq 1$. It reaches $w = 1$ when the radiation is unidirectional along the polar axis of the reference system, while $w = -1/2$ when the radiation field is azimuth-independent and confined to the plane perpendicular to the quantization axis. We have calculated the tensors of the radiation field by using the center-to-limb variation and the wavelength dependence of the solar continuum radiation field tabulated by Pierce (2000). Since the He I lines originate in the outer regions of the solar/stellar atmosphere, it is necessary to take into account the geometrical effect produced by the non-negligible height h above the surface of the star. To this end, we have applied the strategy outlined in §12.3 of Landi Degl’Innocenti & Landolfi (2004). Figure 4 shows the sensitivity of w and \bar{n} to the height in the solar atmosphere at which our slab is assumed to be located. The number of photons per mode decreases, while the anisotropy factor rapidly increases. This effect is of a purely geometrical nature.

It is important to note that the theory of spectral line polarization presented in the monograph of Landi Degl’Innocenti & Landolfi (2004) is only valid if the radiation field illuminating the atomic system is spectrally flat (independent of frequency) over a frequency interval larger than the Bohr frequencies connecting the levels that present quantum coherences. Fortunately, this is the case for all the lines included in the atomic model of Fig. 2, except for the $3p^3P-2s^3S$ transition at 3888.6 \AA which is situated in a quite crowded region of the spectrum. Fortunately, this line is of secondary importance in setting the statistical equilibrium, and according to Landi Degl’Innocenti & Landolfi (2004) the statistical tensors can be calculated by simply reducing the photospheric continuum radiation intensity at that wavelength by a factor 5. In any case, its inclusion has a rather negligible impact on the final results.

3. The forward modeling code

By forward modeling we mean the calculation of the emergent Stokes profiles for given values of the height h at which the slab is located above the visible solar “surface”, of the slab’s optical thickness and of the magnetic field vector. We have written this option of our computer program in a way such that it performs the calculation at various levels of realism. We point out that similar type of forward-modeling calculations can be carried out also with some of the computer programs mentioned in §1, which are likewise based on the density-matrix theory of spectral line polarization. The main difference with ours is that we have taken into account radiative transfer effects (without neglecting the magneto-optical terms of the Stokes-vector transfer equation) and that we have developed a user-friendly interface to facilitate the performing of numerical experiments (see Fig. 5). In what follows we first describe the various options of our computer program and then show some illustrative examples of possible applications.

3.1. Description of the computing options

The solution of the statistical equilibrium equations, using the radiation field tensors calculated from the given illumination conditions, provides the multipolar components of the atomic density matrix. The computer program calculates such $\rho_Q^K(J, J')$ elements in both the magnetic field reference frame (if a deterministic magnetic field is present) and in a reference system where the quantization axis lies along the solar local vertical direction (hereafter, “vertical frame”). This option of the forward modeling code helps to understand what’s going on at the atomic level when an atomic system is subjected to anisotropic radiative pumping processes in the absence and in the presence of a magnetic field. Some illustrative examples for the J -levels involved in the 10830 Å and D₃ transitions are shown in §3.2 below.

The values of the multipolar components of the density matrix is all we need for calculating the coefficients of the emission vector and of the propagation matrix, which enter the Stokes vector transfer equation (1). Our forward modeling code can solve this equation at the various levels of approximation explained in §2.1. Moreover, it can also compute the emergent Stokes profiles calculating the wavelength positions of the π and σ components assuming the linear Zeeman-effect regime (instead of using the general Paschen-Back effect theory), incorporating or discarding the influence of atomic level polarization.

3.2. Atomic level polarization in two reference systems

Figure 6 shows an illustrative example of the population imbalances $[\rho_0^2(J)$ and $\rho_0^1(J)]$ and quantum coherences $[\rho_Q^2(J)$ and $\rho_Q^1(J)$, with $Q \neq 0$] induced by optical pumping processes in the levels of the He I 10830 Å multiplet that can carry atomic polarization (i.e., the lower level, with $J_l = 1$, and the upper levels with $J_u = 2$ and $J_u = 1$). Like in Trujillo Bueno & Asensio Ramos (2007), we assume a slab with $\Delta\tau_{\text{red}} = 1$, where the label “red” indicates that the optical thickness of the slab along its normal direction is measured at the frequency where the peak of the red blended component of the 10830 Å multiplet is located. The slab is assumed to be at a height of only 3 arcseconds and in the presence of a horizontal magnetic field whose strength we can vary at will.

Consider first the results for $J_l = 1$ and $B = 0$ G in a reference system with the quantization axis along the local vertical. Since the pumping radiation is assumed to be unpolarized and with axial symmetry around the vertical, for $B \approx 0$ G we see only population imbalances of the form $\rho_0^2(J)$. Note that in the absence of magnetic fields the $\rho_0^1(J_l)$ atomic orientation value is zero because there is no net circular polarization in the incident radiation field. The bottom right panel of Fig. 6 shows that, for $B = 0$ G, we have lower-level quantum coherences of the form $\rho_Q^2(J)$ (with $Q \neq 0$) in the magnetic reference system, whose Z -axis is inclined with respect to the symmetry axis of the pumping radiation field. In fact, for given illumination conditions in the absence of a magnetic field, whether or not we have such quantum coherences depends only on the reference system. In each of the two bottom panels it is shown what happens with the population imbalances and the coherences of the $J_l = 1$ lower level as the strength of the assumed horizontal field is increased. Consider, for instance, the right panel results corresponding to the magnetic field reference frame. Note that the lower-level Hanle effect starts to operate for field strengths as low as 0.01 G, and that for field intensities of the order or larger than 1 G all the lower-level coherences have been relaxed. This happens because such a lower level is metastable, which implies that its critical Hanle field is only 0.1 G (see Eq. 16). It is also of interest to point out that if the J -levels of our multiterm atomic model were isolated levels then the $\rho_0^2(J)$ population imbalances would be constant in the magnetic field reference frame, and the $\rho_0^1(J)$ atomic orientation value would be zero. However, since the J -levels suffer crossings and repulsions non-zero $\rho_0^1(J)$ values appear through the alignment-to-orientation conversion mechanism (cf. Landi Degl’Innocenti 1982), which for the 10830 Å triplet has however a negligible impact on the emergent Stokes V profiles. In addition, as shown in the bottom right panel, the $\rho_0^2(J_l)$ alignment coefficient itself starts to be modified as soon as the field strength is sensibly larger than 100 G. Although this lower level does not suffer any crossings with the other J -levels of the model atom of Fig. 2, its atomic polarization is modified because it sensitively depends on that of the upper levels of the 10830 Å multiplet.

Consider now the results for the upper levels with $J_u = 1$ (central panels of Fig. 6) and $J_u = 2$ (top panels). Obviously, we only see population imbalances of the form $\rho_0^2(J)$ at zero field in the vertical frame. Around $B = 10^{-2}$ G, the density matrix elements start to be affected by the magnetic field. This modification is due to the feedback effect that the alteration of the lower-level polarization has on the upper levels. It is also possible to note in the central and top panels of Fig. 6 the action of the upper level Hanle effect on the $J_u = 1$ and $J_u = 2$ levels. In fact, there is a hint of a small plateau just above 0.1 G, as expected from the fact that the critical upper-level Hanle field value is 0.8 G for the 10830 Å multiplet (see Table 3). Similar features can be seen in the corresponding right panels of Fig. 6. Probably, the most notable conclusion to highlight from this figure is that between approximately 10 and 100 G we only have population imbalances of the form $\rho_0^2(J)$ in the magnetic field reference frame (i.e., we can consider that between 10 and 100 G the He I 10830 Å multiplet is in the saturation regime of the Hanle effect, where the coherences are negligible and the atomic alignment values of the lower and upper levels are insensitive to the strength of the magnetic field).

Finally, in Fig. 7 we show similar results but for the upper levels of the He I D₃ multiplet. The situation now is much more complicated, as evidenced by the fact that it is impossible to find a range of solar magnetic field strength values between which the coherences are zero in the magnetic field reference frame and, at the same time, the population imbalances are insensitive to the magnetic strength.

3.3. How to investigate empirically the possibility of magnetic canopies in the quiet solar chromosphere?

In the presence of an *inclined* magnetic field forward scattering processes can produce linear polarization signatures in spectral lines (e.g., the review by Trujillo Bueno 2001). In this geometry, the polarization signal is *created* by the Hanle effect, a physical phenomenon that has been clearly demonstrated via spectropolarimetry of solar coronal filaments in the He I 10830 Å multiplet (Trujillo Bueno et al. 2002b).

Fig. 8 shows theoretical examples of the emergent fractional linear polarization in the lines of the He I 10830 Å multiplet assuming a constant-property slab of helium atoms permeated by a horizontal magnetic field of 10 G. As expected, the smaller the optical thickness of the assumed plasma structure the smaller the fractional polarization amplitude. In principle, the Tenerife Infrared Polarimeter (TIP; Martínez Pillet et al. 1999; Collados et al. 2007) mounted on the Vacuum Tower Telescope (VTT) of the Observatorio del Teide allows the detection of very low amplitude polarization signals, such as those corresponding to the

$\Delta\tau_{\text{red}} = 0.1$ case of Fig. 8. However, in order to be able to achieve this goal without having to sacrifice the spatial and/or temporal resolution we need a larger aperture solar telescope.

We consider now the question of whether it is safer to interpret disk-center observations or to opt for a different scattering geometry. To this end, we have investigated how is the variation of Q/I and U/I at the central wavelengths of the red and blue components of the 10830 Å multiplet for different inclinations (θ_B) of the magnetic field vector and for different line-of-sights, assuming $\Delta\tau_{\text{red}} = 0.1$ and $B = 10$ G (which implies that we are very close to the saturation regime of the upper level Hanle effect). Fig. 9 shows only the case of magnetic field vectors with azimuth $\chi_B = 90^\circ$ (i.e., contained in the Z-Y plane of Fig. 1) and for line-of-sights with $\chi = 0$ (i.e., contained in the Z-X plane of Fig. 1). It is interesting to note that for the case of a horizontal magnetic field (i.e., $\theta_B = 90^\circ$, which implies that the magnetic field vector forms always an angle of 90° with respect to any of the line-of-sights of Fig. 9) Stokes $U = 0$ and the Stokes Q amplitudes of the emergent spectral line radiation are identical for all such line-of-sights. This is easy to understand by using the following approximate expressions for ϵ_Q/ϵ_I and η_Q/η_I , which for the case of a deterministic magnetic field provide a suitable approximation if we are in the saturation regime of the upper-level Hanle effect (Trujillo Bueno 2003):

$$\frac{\epsilon_Q}{\epsilon_I} \approx \frac{3}{2\sqrt{2}} (\mu_B^2 - 1) \mathcal{W}[\sigma_0^2(J_u)]_B, \quad (20)$$

$$\frac{\eta_Q}{\eta_I} \approx \frac{3}{2\sqrt{2}} (\mu_B^2 - 1) \mathcal{Z}[\sigma_0^2(J_l)]_B, \quad (21)$$

where $[\sigma_0^2]_B = [\rho_0^2]_B/\rho_0^0$ quantifies the fractional atomic alignment in the magnetic field reference frame, while \mathcal{W} and \mathcal{Z} are numerical coefficients that depend on the J_l and J_u values⁴. It is very important to note that in Eqs. (20) and (21) μ_B is *the cosine of the angle between the magnetic field vector and the line of sight*. Note also that in these expressions for ϵ_Q/ϵ_I and η_Q/η_I , that are valid in the magnetic field reference frame, we have chosen the positive reference direction for Stokes Q parallel to the projection of the magnetic field vector onto the plane perpendicular to the LOS, while in the similar Eqs. (16) and (17) of Trujillo Bueno & Asensio Ramos (2007) we chose it along the perpendicular direction. In both cases, we have $\epsilon_U = \eta_U = 0$ (if we are really in the above-mentioned Hanle-effect saturation regime). Obviously, the observed Q/I amplitude depends on the fractional atomic

⁴Actually, $\mathcal{W} = w_{J_u J_l}^{(2)}$ and $\mathcal{Z} = w_{J_l J_u}^{(2)}$, with $w_{J J'}^{(2)}$, given by Eq. (10.12) of Landi Degl’Innocenti & Landolfi (2004). For instance, $\mathcal{W} = 0$ and $\mathcal{Z} = 1$ for a line transition with $J_l = 1$ and $J_u = 0$, such as that of the blue component of the 10830 Å triplet.

alignment of the upper and lower levels of the 10830 Å line transitions calculated in the magnetic field reference frame, but their values are independent of the LOS. Actually, in the weak anisotropy limit they are given by

$$[\sigma_0^2]_B = [\sigma_0^2]_V \frac{1}{2}(3 \cos^2 \theta_B - 1), \quad (22)$$

where $[\sigma_0^2]_V$ is the fractional atomic alignment in the vertical frame for the zero field case. Therefore, the dependency of the emergent Stokes Q signal on the scattering angle is only through the factor $(\mu_B^2 - 1)$, with $\mu_B = 0$ for all the line-of-sights of Fig. 9 if $\theta_B = 90^\circ$.

As seen in Fig. 9, for non-horizontal fields there are notable differences between the curves corresponding to each LOS, mainly for the cases with an inclination (θ_B) of the magnetic field smaller than the Van-Vleck angle ($\theta_{VV} = 54.73^\circ$, which corresponds to $\cos^2(\theta_{VV}) = 1/3$). For the forward-scattering case of a disk-center observation (the $\mu = 1$ curves of Fig. 9) Stokes $U \approx 0$ and Stokes Q admits only one solution for $\theta_B > \theta_{VV}$ (with the exception of the well-known 180° ambiguity of the Hanle effect)⁵. However, for $\theta_B < \theta_{VV}$ we may have two different magnetic field inclinations producing the same Stokes Q values, each of them having its corresponding 180° ambiguity of the Hanle effect. As seen in the figure, the range of θ_B values where two such solutions for Stokes Q are possible depends on the μ -value of the LOS. Stokes U is clearly non-zero for $\mu < 1$, but the fact that $U \approx 0$ for the case of magnetic field with fixed inclination but with random-azimuth within the spatio-temporal resolution element of the observation, leads us to conclude that the best one can do for a reliable empirical investigation of the possibility of canopy-like fields in the quiet solar chromosphere is to interpret spectropolarimetric observations at the solar disk center, such as those considered in §5.4.

4. The Inversion Code

Our inversion strategy is based on the minimization of a merit function that quantifies how well the Stokes profiles calculated in our atmospheric model reproduce the observed Stokes profiles. To this end, we have chosen the standard χ^2 -function, defined as:

$$\chi^2 = \frac{1}{4N_\lambda} \sum_{i=1}^4 \sum_{j=1}^{N_\lambda} \frac{[S_i^{\text{syn}}(\lambda_j) - S_i^{\text{obs}}(\lambda_j)]^2}{\sigma_i^2(\lambda_j)}, \quad (23)$$

⁵The reason why Stokes U in forward scattering geometry is not exactly zero for the red component is because for B=10 G some of the coherences are not completely insignificant.

where N_λ is the number of wavelength points and $\sigma_i^2(\lambda_j)$ is the variance associated to the j -th wavelength point of the i -th Stokes profiles. The minimization algorithm tries to find the value of the parameters of our model that lead to synthetic Stokes profiles S_i^{syn} with the best possible fit to the observations. For our slab model, the number of parameters (number of dimensions of the χ^2 hypersurface) lies between 5 and 7, the maximum value corresponding to the optically thick case (see Table 1). The magnetic field vector (B , θ_B and χ_B), the thermal velocity (v_{th}) and the macroscopic velocity (v_{mac}) are always required. This set of parameters is enough for the case of an optically thin slab. In order to account for radiative transfer effects, we need to define the optical depth of the slab along its normal direction and at a suitable reference wavelength (e.g., the central wavelength of the red blended component for the He I 10830 Å multiplet). In addition, we may additionally need to include the damping parameter (a) of the Voigt profile if the wings of the observed Stokes profiles cannot be fitted using Gaussian line profiles.

A critical problem in any inversion code is to identify possible degeneracies among different parameters of the model. When two or more parameters produce similar effects on the emergent Stokes profiles, the inversion algorithm is unable to distinguish between them. As a result, the emergent Stokes profiles corresponding to different combinations of the model parameters are indistinguishable within the noise level. Concerning this critical point, we investigate in detail in §6.2 the possibility of using the observed Stokes profiles of the 10830 Å triplet to obtain the value of the height h at which the observed plasma structure is located.

Ambiguities in the determination of the model’s parameters can also result from the presence of degeneracies. However, this type of ambiguities occur only for a finite number of combinations of some parameters. Although the problem is complicated, it is possible to develop techniques that can help selecting one of the combinations as the most plausible. The well-known 180° ambiguity of the Hanle effect adds to the unfamiliar Van Vleck ambiguity (House 1977; Casini & Judge 1999; Casini et al. 2005; Merenda et al. 2006). The role of these ambiguities in the inferred model’s parameters will be explored in §6.1, although some hints have been already given in §3.3.

It is also important to point out the interest of developing methods capable of providing reliable confidence intervals for all the inferred parameters. In a future development, we plan to implement Bayesian inference techniques (Asensio Ramos et al. 2007).

4.1. Levenberg-Marquardt

Probably, the most well-known procedure for the minimization of the χ^2 -function is the Levenberg-Marquardt (LM) method (e.g., Press et al. 1986). The minimization strategy uses the Hessian method when the parameters are close to the minimum of the χ^2 -function (a quadratic form approximately describes this function around the minimum) and the steepest descent method when the parameters are far from the minimum. The transition between both methods is done in an adaptive manner. Its main drawback (which applies also to the majority of the standard numerical methods of function minimization) is that it can easily get trapped in local minima of the χ^2 -function. Some alternatives are available to overcome this difficulty. The most straightforward but time consuming one is to restart the minimization process at different values of the initial parameters. If the obtained minimum is systematically the same, the probability that this is the global optimum is high. However, when the χ^2 parameter hypersurface is complicated, this technique does not give any confidence on the validity of the global minimum. Other possibilities rely on the application of some kind of “inertia” to the method, so that the LM method can overcome such a local minimum problem when moving on the parameter hypersurface. Again, these methods do not guarantee the success of getting the global minimum of the function. On the contrary, the LM method turns out to be one of the fastest and simplest options when the initial estimate of the parameters is close to the absolute minimum.

4.2. Global Optimization techniques

In order to avoid the possibility of getting trapped in a local minimum of the χ^2 hypersurface, global optimization methods have to be used. Several optimization methods have been developed to obtain the global minimum of a function (e.g., Horst & Pardalos 1995). The majority of them are based on stochastic optimization techniques. The essential philosophy of these methods is to sample efficiently the whole space of parameters to find the global minimum of a given function. One of the most promising methods is genetic optimization (inspired by the fact of biological evolution), in which the parameters of the merit function are encoded in a gene. Although no mathematical proof of the convergence properties of these algorithms exists, recent advances suggest that the probability of convergence is very high (Gutowsky 2004). Actually, they perform quite well in practice for the optimization of very hard problems. In solar spectropolarimetry, genetic optimization methods have been recently applied by Lagg et al. (2004) to the inversion of Stokes profiles induced by the Zeeman effect in the He I 10830 Å triplet, neglecting the influence of atomic level polarization. The main disadvantage is that the computing time needed to reach con-

vergence increases dramatically (by a factor ~ 10 with respect to standard methods based on the gradient descent like LM).

Another different approach is based on deterministic algorithms (Horst & Pardalos 1995). Typically, these algorithms rely on a strong mathematical basis, so that their convergence properties are well known. We have chosen the DIRECT algorithm (Jones et al. 1993), whose name derives from one of its main features: *dividing rectangles*. The idea is to recursively sample parts of the space of parameters, improving in each iteration the location of the part of the space where the global minimum is potentially located. The decision algorithm is based on the assumption that the function is Lipschitz continuous (see Jones et al. 1993, for details). The method works very well in practice and can indeed find the minimum in functions that do not fulfill the condition of Lipschitz continuity. The reason is that the DIRECT algorithm does not require the explicit calculation of the Lipschitz constant but it uses all possible values of such a constant to determine if a region of the parameter space should be broken into subregions because of its potential interest (see Jones et al. 1993, for details). A schematic illustration of the subdivision process for a function of two parameters is shown in Fig. 10.

4.3. Convergence

Taking into account that the dimension of our space of parameters is between 5 and 7, it seems unreasonable to use an algorithm like DIRECT to obtain a precise determination of the values of the model’s parameters at the global minimum. The reason is that the precision in the values of the parameters decreases with the size of the hyperrectangles. Therefore, we would need to perform many divisions to end up with a reasonable precision. What we do is to let the DIRECT algorithm locate the global minimum in a region whose hypervolume is V . This hypervolume is obtained as the product of the length d_i of each dimension associated with each of the N parameters:

$$V = \prod_i^N d_i. \tag{24}$$

When the hypervolume decreases by a factor f after the DIRECT algorithm has discarded some of the hyperrectangles, its size along each dimension is approximately decreased by a factor $f^{1/N}$. In order to end up with a small region where the global minimum is located, many subdivisions are necessary, thus requiring many function evaluations. For this reason, it has been observed that although the DIRECT algorithm rapidly finds the region where the global minimum is located, its local convergence properties are rather poor (see, e.g., Cox et al. 2001; Bartholomew-Biggs et al. 2002; Ljungberg et al. 2004, for applications in

the extremely hard problems of the design of high-speed civil transport, aircrafts and bioinformatics). In summary, the DIRECT method is an ideal candidate for its application as an estimator of the region where the global minimum is located, but not for determining it.

The most time consuming part of any optimization procedure is the evaluation of the merit function. The DIRECT algorithm needs only a reduced number of evaluations of the merit function to find the region where the global minimum is located. For this reason, we have chosen it as the initialization part of the LM method. Since the initialization point is close to the global minimum, the LM method, thanks to its quadratic behavior, rapidly converges to the minimum.

4.4. Stopping criterium

A critical and fundamental problem in the optimization of functions (either local or global) is to identify when the method has converged to the solution. We have used two stopping criteria for the DIRECT algorithm. The first one is stopping when the ratio between the hypervolume where the global minimum is located and the original hypervolume is smaller than a given threshold. This method has been chosen when using the DIRECT algorithm as an initialization for the LM method, giving very good results. The other good option, suggested by Jones et al. (1993), is to stop after a fixed number of evaluations of the merit function.

Since the intensity profile is not very sensitive to the presence of a magnetic field (at least for magnetic field strengths of the order of or smaller than 1000 G), we have decided to estimate the optical thickness of the slab, the thermal and the macroscopic velocity of the plasma and the damping constant by using only the Stokes I profile, and then to determine the magnetic field vector by using the polarization profiles. The full inversion scheme, shown schematically in Table 2, begins by applying the DIRECT method to obtain a first estimation of the indicated four parameters by using only Stokes I . Afterwards, some LM iterations are carried out to refine the initial values of the model’s parameters obtained in the previous step. Once the LM method has converged, the inferred values of v_{th} , v_{mac} (together with a and $\Delta\tau$, when these are parameters of the model) are kept fixed in the next steps, in which the DIRECT method is used again for obtaining an initial approximation of the magnetic field vector (B, θ_B, χ_B) . According to our experience, the first estimate of the magnetic field vector given by the DIRECT algorithm is typically very close to the final solution. Nevertheless, some iterations of the LM method are performed to refine the value of the magnetic field strength, inclination and azimuth. In any case, although we have found very good results with this procedure, the specific inversion scheme is fully configurable and can be tuned for

specific problems.

5. Applications

The main aim of this section is to illustrate the application of our inversion code to some selected spectropolarimetric observations in the He I 10830 Å multiplet, showing that it gives results that are in agreement with the published ones. In addition, in §5.4 we show a new application aimed at determining the strength and inclination of the magnetic field vector in the chromosphere above an internetwork region observed at solar disk center. Note that in the following applications $\Delta\tau_{\text{red}}$ will continue denoting the optical thickness of the constant-property slab, along its normal direction, measured at the center of the red blended component of the He I 10830 Å multiplet.

5.1. Prominences

The first application is for the case of solar prominences, which are relatively cool and dense plasma structures embedded in the $T \sim 10^6$ K solar corona. In these objects the observed Stokes Q and U profiles of the He I 10830 Å multiplet are dominated by the presence of atomic level polarization, while the Stokes V profile is dominated by the Zeeman effect. Recently, Merenda et al. (2006) have shown how to infer the magnetic field that confines the plasma of solar prominences via the inversion of the Stokes profiles induced by scattering processes and the Hanle and Zeeman effects in the lines of the He I 10830 Å multiplet. They analyzed in detail spectropolarimetric observations of the He I 10830 Å multiplet in a polar crown prominence and concluded that if the observed prominence was located in the plane of the sky the magnetic field had to be relatively strong ($B \approx 30$ G) and inclined by only 25° with respect to the local vertical.

We have applied our inversion code to the spectropolarimetric observations shown in Fig. 11, taken from Fig. 9 of Merenda et al. (2006). We have assumed that the observed plasma structure was optically thin and that the prominence is located in the plane of the sky. The inversion code was used to infer the value of the thermal velocity v_{th} , the macroscopic velocity shift v_{mac} (to allow for a shift in the wavelength calibration) and the magnetic field vector (B, θ_B, χ_B) . The atmospheric height was fixed to $h = 20''$, the same value used by Merenda et al. (2006). After the four steps summarized in Table 2, we end up with a thermal velocity $v_{\text{th}} = 7.97 \text{ km s}^{-1}$, a bulk velocity that is compatible with zero and a magnetic field vector characterized by $B = 26.8$ G, $\theta_B = 25.5^\circ$ and $\chi_B = 161.0^\circ$. These values are in very

good agreement with the results of Merenda et al. (2006), namely $B = 26$ G, $\theta_B = 25^\circ$ and $\chi_B = 160.5^\circ$. Note that since the prominence plasma was assumed to lie in the plane of the sky, the following solutions are also valid: $\theta_B^* = 180^\circ - \theta_B$ and $\chi_B^* = -\chi_B$ (i.e., the well-known 180° ambiguity of the Hanle effect).

We point out that the total number of evaluations of the merit function was 132. For the inversion of the Stokes profiles corresponding to other points of the field of view, one can initialize the inversion using the model’s parameters corresponding to the previous point. Using a few LM iterations, one should be able to reach the global minimum. In case this procedure does not work properly, one should return to the four-steps inversion scheme already presented in Table 2.

5.2. Spicules

Another interesting problem is the determination of the magnetic field vector in solar chromospheric spicules. Trujillo Bueno et al. (2005) interpreted spectropolarimetric observations of spicules in the He I 10830 Å multiplet and concluded that the magnetic field of spicules in quiet regions of the solar chromosphere has a strength of the order of 10 G and is inclined by about 35° with respect to the local vertical. Their conclusion that the typical magnetic field strength is ~ 10 G required to obtain the longitudinal component of the magnetic field vector via some careful measurements of the Stokes V profiles, such as that shown in Fig. 13 of Trujillo Bueno (2005). This was needed because for field strengths larger than a few gauss the He I 10830 Å multiplet enters the saturation regime of the upper-level Hanle effect and the observed Stokes Q and U profiles provide only information on the orientation of the magnetic field vector. In fact, the application of our inversion code to the observed Stokes profiles shown in Fig. 12 (where the Stokes V profile is at the noise level), assuming that the spicular material is located in the plane of the sky, provides several different magnetic field vectors that lead to equally reliable fits. One of them, given by $B = 10$ G, $\theta_B = 37^\circ$ and $\chi_B = 172^\circ$ is similar to the one chosen by Trujillo Bueno et al. (2005). Another possible fit is the one illustrated in Fig. 12, which corresponds to $B = 2.6$ G, $\theta_B = 37^\circ$ and $\chi_B = 35^\circ$.

Fig. 13 gives the values of the χ^2 function for all possible magnetic field inclinations and azimuths corresponding to the cases $B = 10$ G (left panel) and $B = 2.6$ G (right panel). In each of these panels we have indicated with white dots and numbers the four solutions that correspond to equally good best fits to the observed Stokes profiles of Fig. 12. The

pair of solutions 1 and 2 correspond to the Van-Vleck ambiguity⁶. The same applies to the 1' and 2' solutions. On the contrary, the pair of solutions 1 and 1' or the 2 and 2' are not strictly equivalent. The inversion code considers such pairs of solutions as equivalent because the observed Stokes V profile is at the noise level and it is not able to differentiate between the two cases. Note that these pairs of solutions give exactly the same Stokes Q and U profiles, but their corresponding Stokes V profiles have opposite signs. Concerning each pair of solutions in Fig. 13, it is possible to verify that the projections on the plane of the sky of the magnetic fields corresponding to solutions 1 and 2 form an angle close to 90° , which is typical of the Van-Vleck ambiguity. The same happens for the magnetic fields corresponding to solutions 1' and 2'. This holds for both cases, $B = 10$ G and $B = 2.6$ G. As pointed out above, when the observed Stokes V signal is very small, it is very hard (or impossible) to differentiate between the two possibilities having azimuths χ_B and $180^\circ - \chi_B$. The magnetic field vectors 1 and 1' (or those corresponding to the 2 and 2' solutions of Fig. 13) have the same projection on the line of sight, except for a sign change. Therefore, the detection of Stokes V turns out to be fundamental to determine which is the correct one (Trujillo Bueno et al. 2005; Merenda et al. 2006). Apart from the considered solutions, which are restricted to the interval $0^\circ < \theta_B < 180^\circ$, one has also to take into account the well-known ambiguity of the Hanle effect, which applies when the emitting plasma is located in the plane of the sky. In this case, we have to add to the possible set of solutions all the combinations fulfilling $\theta_B^* = 180^\circ - \theta_B$ and $\chi_B^* = -\chi_B$ since both pairs produce the same Stokes profiles.⁷.

5.3. Filaments

We have also considered the inversion of the Stokes profiles presented in Trujillo Bueno et al. (2002b), which were observed in a solar coronal filament at the solar disk center. Such profiles, which are reproduced in Fig. 14, were used by those authors to demonstrate the presence of atomic polarization in the lower level of the 10830 Å multiplet and that the

⁶Information on this ambiguity, typical of the Hanle-effect saturation regime, can be found in Casini et al. (2005), in Merenda et al. (2006) and in §6.1 below.

⁷We point out that this ambiguity of the Hanle effect applies only to some particular scattering geometries (i.e., to those of 90° and of forward scattering). If the observed plasma structure is not located in the plane of the sky (which implies scattering processes at an angle different from 90°), or if it is not located at the solar disk center, then one has a sort of quasi-degeneracy which can disappear when the angle θ of Fig. 1 is considerably different from 90° or from 0° . This fact has been exploited by Landi Degl'Innocenti & Bommier (1993) to propose a method for removing the azimuth ambiguity intrinsically present in vector magnetograms.

Hanle effect due to an inclined magnetic field creates linearly polarized radiation in forward scattering geometry. Note that the Stokes Q , U and V profiles are normalized to the maximum depression in Stokes I (which is $0.4 I_c$, approximately). The application of our inversion code using $h = 40''$ confirms the conclusions of Trujillo Bueno et al. (2002b), yielding the following values for the model’s parameters: $\Delta\tau = 0.86$, $v_{\text{th}} = 6.6 \text{ km s}^{-1}$, $a = 0.19$ and a magnetic field vector characterized by $B = 18 \text{ G}$ and $\theta_B = 105^\circ$.

5.4. Inter-network regions

As discussed in §3.3, the investigation of the possibility of horizontal magnetic canopies in the quiet solar chromosphere above internetwork regions is feasible with TIP, especially when interpreting measurements of the polarization of the He I 10830 Å multiplet in forward scattering at the solar disk center⁸. We present in Fig. 15 an observation carried out with TIP very close to the solar disk center ($\mu = 0.98$). The slit was crossing an enhanced network region of circular shape. A time series of 50 steps with an integration time of 3 seconds was performed. The resulting polarimetric sensitivity after averaging over the 50 time steps and along a small spatial interval within the observed internetwork region is close to 6×10^{-5} in units of the continuum intensity. According to the results of the right panel of Fig. 8, this is sufficient for detecting the linear polarization signal of a horizontal magnetic field provided the optical depth at the wavelength of the red component of the 10830 Å multiplet is larger than ~ 0.01 . The reference system has been rotated until Stokes U is minimized. Since the inferred magnetic field strength implies that the He I 10830 Å is in the saturation regime of the upper-level Hanle effect, the resulting reference direction for Stokes Q lies either along the projection of the magnetic field vector on the solar disk, or along the direction perpendicular to such a projection. We have applied our inversion code to the above-mentioned observed profiles assuming a slab located at a height of 3 arcsec and we have obtained the following results: $\Delta\tau = 0.19$, $v_{\text{th}} = 9.2 \text{ km s}^{-1}$, $a = 0.62$ and a magnetic field vector characterized by $B = 35 \text{ G}$, $\theta_B = 21^\circ$ and $\chi_B = 0^\circ$. However, other possible solutions can be found with a similar goodness of the fit (e.g., $B = 47 \text{ G}$, $\theta_B = 47^\circ$ and $\chi_B = 0^\circ$). These results obtained from a solar disk center observation suggest the presence of magnetic fields inclined by no more than 50° in the observed quiet Sun chromospheric region.

⁸For a preliminary interpretation of an observation of a quiet region located at $\mu = 0.5$ see Lagg (2007).

5.5. Emerging magnetic flux regions

As pointed out by Trujillo Bueno & Asensio Ramos (2007), the modeling of the emergent Stokes Q and U profiles of the He I 10830 Å multiplet should be done by taking into account the possible presence of atomic level polarization, even for magnetic field strengths as large as 1000 G. An example of a spectropolarimetric observation of an emerging magnetic flux region is shown by the circles of Fig. 16. The solid lines show the best theoretical fit to these observations of Lagg et al. (2004). Here, in addition to the Zeeman effect, we took into account the influence of atomic level polarization. The dotted lines neglect the atomic level polarization that is induced by anisotropic radiation pumping in the solar atmosphere. Our results indicate the presence of atomic level polarization in a relatively strong field region (~ 1000 G). However, it may be tranquilizing to point out that both inversions of the observed profiles yield, at least for this case, a similar magnetic field vector, in spite of the fact that the corresponding theoretical fit is much better for the case that includes atomic level polarization.

6. Ambiguity and degeneracies

In the previous subsections we have shown how our inversion code can be used for recovering the parameters of the assumed slab atmospheric model from the Stokes profiles observed in different solar plasma structures. The aim of this section is to discuss the Van Vleck ambiguity and to investigate whether we can infer the height of the observed plasma structure directly through the inversion approach.

6.1. Van Vleck Ambiguity

In general, the solution to any inversion problem is not unique –that is, it is often possible to detect several solutions which are compatible with the observations (e.g., Asensio Ramos et al. 2007). Some of the unicity problems are associated with the physics of the polarization phenomena (e.g., the 180° ambiguity of the Hanle effect for plasma structures located in the plane of the sky or the Van Vleck ambiguity). However, as seen in §5.2, in addition to this type of ambiguities, other degeneracies can appear because of the presence of noise in the observed Stokes profiles.

The Van Vleck ambiguity occurs only for some combinations of the inclinations and azimuths. Moreover, it occurs mainly in the saturation regime of the Hanle effect. For example, Fig. 6 of Merenda et al. (2006) shows the region of parameters for which the Van

Vleck ambiguity occurs in the Hanle-effect saturation regime of the He I 10830 Å triplet. Since two different magnetic field vectors give rise to exactly the same emergent Stokes profiles, it is impossible to distinguish between them using only the 10830 Å multiplet (or four solutions, if the 180° ambiguity of the Hanle effect also applies). However, if more information is introduced in the inversion procedure (for instance, by using simultaneous observations in the 10830 Å and D₃ multiplets), it might be possible to distinguish between the two possible solutions.

Unfortunately, it is not easy to determine the range of parameters in which we may have the Van Vleck ambiguity. One possibility (used by Merenda et al. 2006) is to consider the theoretical Hanle diagram of the red line of the He I 10830 Å multiplet and detect if the observed profiles fall in the ambiguity region. We propose another method based on the DIRECT algorithm implemented in our inversion code. The DIRECT algorithm can rapidly detect regions of the space of parameters where the global minimum may be located. Therefore, we can take advantage of this property to identify the two (or more) points in the space of parameters (θ_B, χ_B) that produce the same emergent Stokes profiles for a given magnetic field strength.

To this end, we have calculated the synthetic emergent Stokes profiles of the He I 10830 Å line from an optically thin prominence, located in the plane of the sky, with $v_{\text{th}} = 8$ km s⁻¹, $h = 20''$, $B = 25$ G, $\theta_B = 40^\circ$ and $\chi_B = 19^\circ$. According to the Hanle diagram shown by Merenda et al. (2006), these profiles are indistinguishable from the ones given by the combination $B = 22$ G, $\theta_B = 100^\circ$ and $\chi_B = 46^\circ$. To these two combinations, we have to add those corresponding to the 180° ambiguity: $(B = 25$ G, $\theta_B = 140^\circ$, $\chi_B = -19^\circ)$ and $(B = 22$ G, $\theta_B = 80^\circ$, $\chi_B = -46^\circ)$. Using the standard four steps inversion procedure explained in §4, the global minimum is rapidly located at position $B = 22$ G, $\theta_B = 100^\circ$ and $\chi_B = 46^\circ$. Keeping fixed the value of all the thermodynamical properties and the field strength, the DIRECT algorithm is used to recover the inclination and azimuth of the magnetic field vector. We show in Fig 17 the position in the (θ_B, χ_B) space of parameters of the N evaluations performed by the DIRECT method. It has been possible to detect the two combinations of parameters that give the same emergent Stokes profiles, as stated above. With only $N = 100$ evaluations of the merit function, the DIRECT algorithm has located and refined the position of the global minimum. It has also identified the second possible solution. When the number of function evaluations increases (even with only $N = 200$), the DIRECT algorithm rapidly locates the two minima. For $N > 200$, we face a degradation in the convergence rate as discussed in §4.3.

As already discussed, an interesting property of the DIRECT method is that no hyper-rectangle is ever discarded from the search. Therefore, a rectangle that in one iteration is

not considered to be potentially interesting, can be chosen for division in a later iteration⁹. This behavior is shown in Fig. 17. When $N = 100$, only a part of the space of parameters has been sampled, with clear gaps for inclinations above 110° . In spite of these gaps, the two global minima have been already found. However, when the number of function evaluation is increased, the numerical scheme finally evaluates the function in those regions with the aim of discarding the presence of additional global minima.

6.2. Can we infer the height of the observed plasma structure?

In this section we briefly discuss the possibility of determining the height at which the He I atoms are located by only using the information contained in the Stokes profiles of the 10830 Å multiplet. For simplicity, we consider first the optically thin limit, the case of off-limb observations (i.e., 90° scattering geometry) and a magnetic field with a fixed azimuth and strength. The synthetic profiles correspond to the case $v_{\text{th}} = 8 \text{ km s}^{-1}$ and $h = 20''$, with the magnetic field vector given by $B = 25 \text{ G}$, $\theta_B = 40^\circ$ and $\chi_B = 19^\circ$. The aim of this experiment is to infer the inclination θ_B and height h from synthetic Stokes profiles without noise. The positions where the merit function has been evaluated by the DIRECT algorithm are presented in the upper panels and in the bottom left panel of Fig. 18. The χ^2 surface is shown in the bottom right panel of Fig. 18. The presence of the vertical strip where the minimum is located makes it very difficult to converge to the minimum using gradient-based methods like the LM method. The derivatives cannot be correctly approximated when the χ^2 function has a large variation in such a small region of the space of parameters. This shallow strip is produced by the quasi-degeneracy of the problem in both parameters. An infinity of combinations of both parameters give Stokes profiles that can approximately reproduce the observations. The difference in the χ^2 merit function between these spurious cases and the exact one is very small. Two reasons produce such a behavior. On the one hand, the linear polarization signal is enhanced when the height is increased because the anisotropy of the radiation field increases (see Fig. 4, right panel). On the other hand, the Hanle effect turns out to be particularly efficient in reducing the atomic polarization when the magnetic field is significantly inclined with respect to the symmetry axis of the radiation field (the vertical direction). In a realistic case, the problem is much more complicated due to the presence of other additional parameters and the noise contamination.

When the observed structure is off the limb, imaging techniques can be used to esti-

⁹This proves to be fundamental to demonstrate that the global minimum will always be found (Jones et al. 1993).

mate h . On the contrary, the case of on-disk observations is much more complicated since no straightforward technique for estimating the height is available. One possibility is to follow the observed active region until it approaches the limb. The height can then be estimated if we assume that the height of the plasma structure has not changed between both observations. An even less precise procedure is to assume a given h value based on the typical height of the solar structure type under study. Obviously, the ideal situation would be the one where h could be inferred directly from the observed Stokes profiles. In order to investigate this possibility, we have performed an experiment in which the DIRECT method is used with disk-center ($\theta = 0^\circ$) synthetic Stokes profiles. The emergent profiles have been calculated with $v_{\text{th}} = 8 \text{ km s}^{-1}$, $\Delta\tau = 0.8$, $h = 20''$, $B = 25 \text{ G}$, $\theta_B = 40^\circ$ and $\chi_B = 19^\circ$, taking into account the effects of radiative transfer in the slab. We keep fixed all the parameters except for the inclination of the magnetic field θ_B and the height h . The upper panels and the bottom left panel of Figure 19 present the points at which the DIRECT algorithm has evaluated the merit function, showing that it is possible to infer the height of the observation by only using the Stokes profiles. The shape of the χ^2 surface is shown in the bottom right panel of Fig. 19. In comparison with the off-limb case shown in Fig. 18, the minimum is located in a much less complicated region of the χ^2 surface. The quasi-degeneracy present in the off-limb case is not present in the on-disk case. This is associated with the fact that the blue component gives no signal in the optically thin limit, while it does if an inclined field is present for the disk center case (Trujillo Bueno et al. 2002b).

Interestingly, if one wants to infer the magnetic field vector and the height simultaneously from the observations, the code is unable to get a suitable global minimum, even in the noiseless case. However, an easily accessible global minimum exists when one of the parameters is kept fixed, thus inferring only the following combinations of parameters: (B, θ_B, h) , (B, χ_B, h) and (θ_B, χ_B, h) .

7. Conclusions

The physical interpretation of spectropolarimetric observations of lines of neutral helium, such as those of the 10830 Å and D₃ multiplets, represents a very important diagnostic window for investigating the dynamical behavior and the magnetic field of plasma structures in the solar chromosphere and corona, such as spicules, filaments, regions of emerging magnetic flux, network and internetwork regions, sunspots, flaring regions, etc. In order to facilitate this type of investigations we have developed a powerful forward modeling and inversion code that permits either to calculate the emergent spectral line intensity and polarization for any given magnetic field vector or to infer the dynamical and magnetic properties

from the observed Stokes profiles. This diagnostic tool is based on the quantum theory of spectral line polarization (see Landi Degl’Innocenti & Landolfi 2004), which self-consistently accounts for the presence of atomic level polarization and the Hanle and Zeeman effects in the most general situation of the incomplete Paschen-Back effect regime. It is also of interest to mention that the same computer program can be easily applied to other chemical species apart from He I (e.g., in order to investigate the magnetic sensitivity of the polarization caused by the joint action of the Hanle and Zeeman effects in many other spectral lines of diagnostic interest, both in the solar atmosphere and in other astrophysical plasmas).

The influence of radiative transfer on the emergent spectral line radiation is taken into account by solving the Stokes-vector transfer equation in a slab of constant physical properties, including the magneto-optical terms of the propagation matrix. Although this “cloud” model for the interpretation of polarimetric observations in such lines of He I is suitable for inferring the magnetic field vector of plasma structures embedded in the solar chromosphere and corona, there are several interesting improvements and generalizations on which we are presently working on. The first one will be useful for improving the modeling of the Stokes profiles observed in low-lying optically-thick plasma structures embedded in the solar chromosphere, such as those of active region filaments. It consists in taking into account that in optically-thick plasma structures located at low atmospheric heights, the atomic level polarization is not going to be necessarily dominated by the anisotropic continuum radiation coming from the underlying solar photosphere (as we have assumed here), given that the radiation field generated by the optically-thick structure itself will tend to reduce the anisotropy factor of the true radiation field that pumps the helium atoms of the plasma structure under consideration (see Trujillo Bueno & Asensio Ramos 2007). The second additional development consists in considering a Milne-Eddington atmospheric model, but determining consistently the height-dependent atomic level polarization induced by the anisotropic radiation field within the atmosphere model that provides the best fit to the observed Stokes profiles. Since the anisotropy factor is very sensitive to the source-function gradient (e.g., Fig. 4 in Trujillo Bueno 2001) the solution of these type of problems in stratified model atmospheres may be facilitated by the application of efficient iterative schemes, such as those used by Manso Sainz & Trujillo Bueno (2003a,b) for developing a general multilevel radiative transfer program for modeling scattering line polarization and the Hanle effect in weakly magnetized stellar atmospheres.

For the solution of the Stokes inversion problem we have applied an efficient algorithm based on global optimization methods, which permits a fast and reliable determination of the global minimum and facilitates the determination of the solutions corresponding to the unfamiliar Van-Vleck ambiguity. Our inversion approach is based on the application of the Levenberg-Marquardt (LM) method for locating the minimum of the merit function

that quantifies the goodness of the fit between the observed and synthetic Stokes profiles. However, gradient-based methods suffer from convergence problems when the initial value of the parameters is not close to the minimum. In order to improve the convergence properties of the LM method, we have introduced a novel initialization technique. This method is based on the DIRECT algorithm, a deterministic global optimization scheme that performs very well. We have shown that a four-steps scheme using the DIRECT method to initialize the parameters and the LM method to refine the first estimation close to the minimum leads to a very robust technique.

Our computer program has been developed with the aim of being computationally efficient and user-friendly. The relevant equations of the problem result from a general and robust theory, so that it is straightforward to treat limiting cases and include or discard several physical effects in a very transparent way. It is appropriate for its application to a wide variety of problems, from simple Zeeman-dominated Stokes profiles to more complex situations in which the influence of atomic level polarization cannot be neglected. The code is written in FORTRAN 90, and incorporates a user-friendly front-end based on IDL¹⁰ which facilitates the execution and analysis of the synthesis and/or inversion calculations (see Fig. 5).

Obviously, our inversion strategy cannot compete in speed with algorithms based on look-up tables, like those applied by Casini et al. (2003) and Merenda et al. (2006). At present, with a modern portable computer, we need of the order of 1 min. for the inversion of the Stokes profiles shown in Fig. 15. The strength of our approach is that it is very general and robust, and very suitable also to investigate the impact of the different physical mechanisms and parameters on the retrieved models. Concerning future improvements, we think that it would be worthwhile to treat the inversion problem within the framework of Bayesian inference techniques (see Asensio Ramos et al. 2007, for a first application of such techniques to the inference of Milne-Eddington parameters from Stokes profiles induced by the Zeeman effect). The aim is to sample the joint posterior probability distribution of the parameters of the model once the observation has been taken into account, and to carry out marginalizations to infer the probability distribution of each parameter. One of the main obstacles to overcome is to determine how to sample efficiently the full posterior probability distribution in the complex physical problem that we have investigated in this paper. A possible solution could be to rely on machine learning techniques for a fast solution of the forward problem, something that could be in perfect synergy with Markov Chain Monte Carlo methods (MacKay 2003).

¹⁰<http://www.itervis.com/idl>

The reliability of the developments presented in this paper has been demonstrated through several model calculations and applications. Of particular interest is the investigation described in Section 3.4, which aimed at clarifying which is the optimum strategy for determining, from He I 10830 Å spectropolarimetric observations, whether or not we have magnetic canopies with horizontal fields in the quiet solar chromosphere. The results of an application to an observation of a disk-center internetwork region can be found in §5.4, which suggest the presence of magnetic fields inclined by no more than 50° in the observed quiet chromospheric region.

We have also discussed the potential problems that one may encounter. For example, we have investigated the presence of degeneracies, paying particular attention to the possibility of determining the height of the observed plasma structure from the observed Stokes profiles themselves and to demonstrate that the DIRECT method is a very efficient technique for detecting the solutions associated to the Van Vleck ambiguity.

“HAZEL” (an acronym from HANle and ZEeman Light) is the name we have given to our IAC computer program for the synthesis and inversion of Stokes profiles resulting from the joint action of the Hanle and Zeeman effects in slabs of finite optical thickness. HAZEL will be continuously improved over the years (e.g., with extensions to more complicated radiative transfer models), but is now ready for systematic applications to a variety of spectropolarimetric observations in the spectral lines of the He I 10830 Å and D₃ multiplets. We offer it to the astrophysical community with the hope that it will help researchers to achieve new breakthroughs in solar and stellar physics. To get a copy, it suffices with making an e-mail request to the authors of this paper.

Acknowledgments We thank Roberto Casini (HAO) for carefully reviewing of our paper. Financial support by the Spanish Ministry of Education and Science through project AYA2007-63881 and by the European Commission through the SOLAIRE network (MTRN-CT-2006-035484) is gratefully acknowledged.

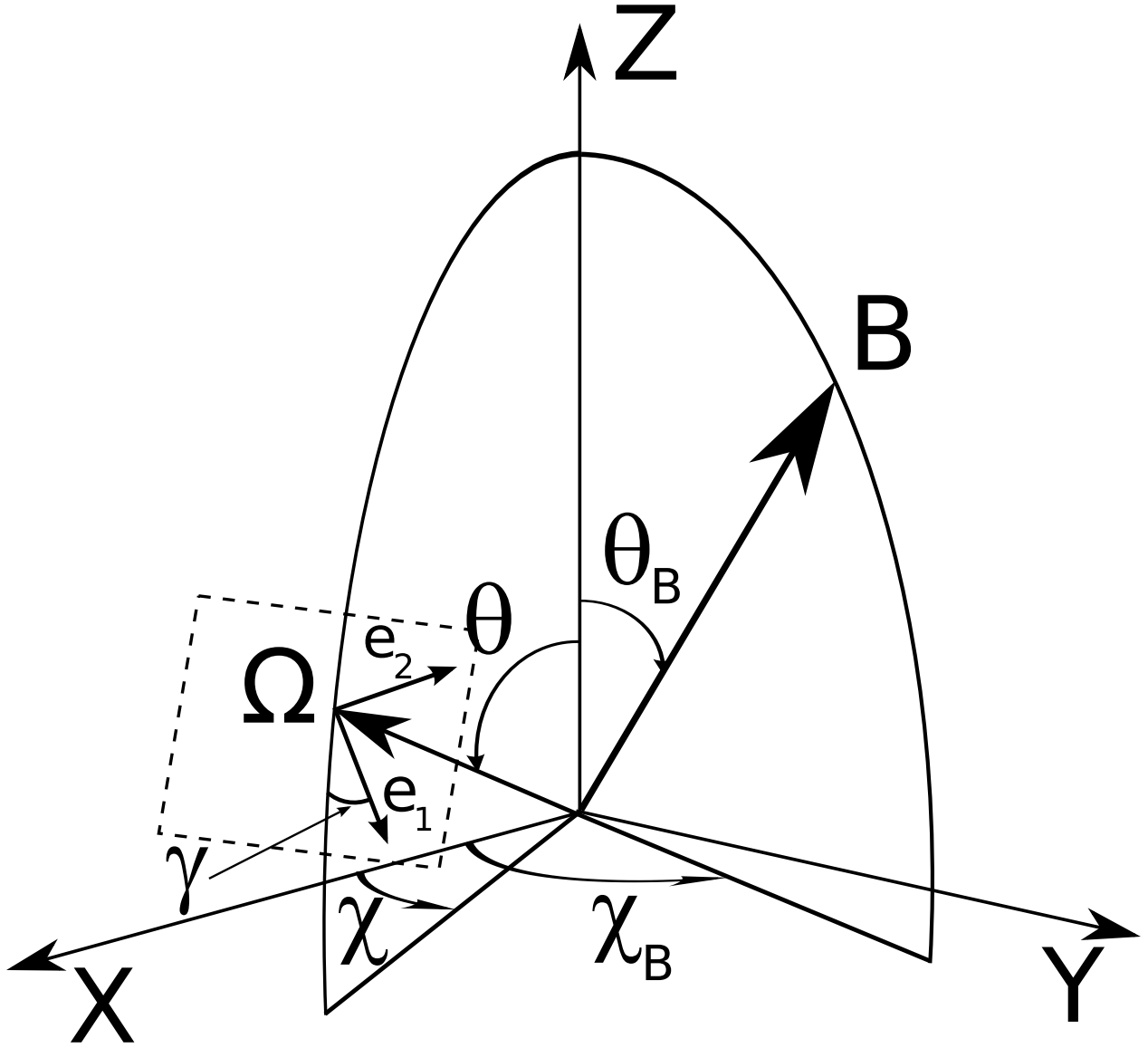


Fig. 1.— The geometry for the scattering event. The Z -axis is placed along the vertical to the solar atmosphere. The magnetic field vector, \mathbf{B} , is characterized by its modulus B , the inclination angle θ_B and the azimuth χ_B . The line-of-sight, indicated by the unit vector $\mathbf{\Omega}$, is characterized by the two angles θ and χ . The reference direction for Stokes Q is defined by the vector \mathbf{e}_1 on the plane perpendicular to the line-of-sight. This vector makes an angle γ with respect to the plane formed by the vertical and the line-of-sight. In the figures showing examples of the emergent Stokes profiles, our choice for the positive reference direction for Stokes Q is $\gamma = 90^\circ$, unless otherwise stated. For off-limb observations, we have $\theta = 90^\circ$, while for observations on the solar disk, we have $\theta < 90^\circ$. Note also that χ is generally taken to be 0° .

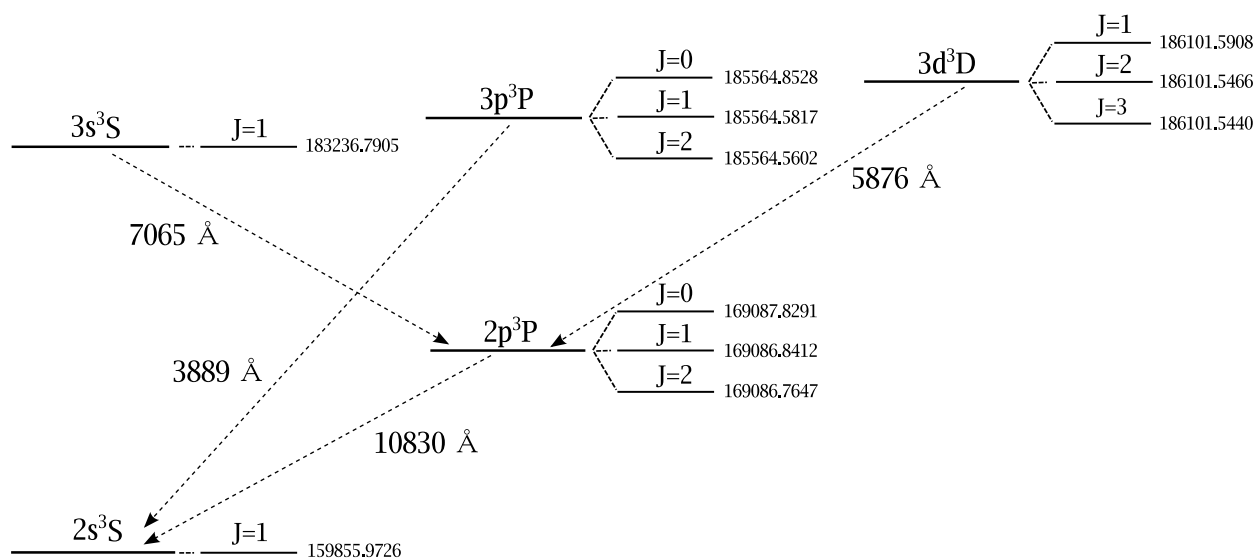


Fig. 2.— Model atom of the triplet system of He I used in this investigation. This work focuses on the polarization properties of the 10830 Å multiplet between the 2p³P and 2s³S terms and on the D₃ multiplet between the 3d³D and 2p³P terms. The energy of each J -level is taken from Drake & Martin (1998) and it is given in cm⁻¹ above the fundamental energy level (1s² ¹S₀). Note that the separation between the J -levels pertaining to each term is not drawn to scale.

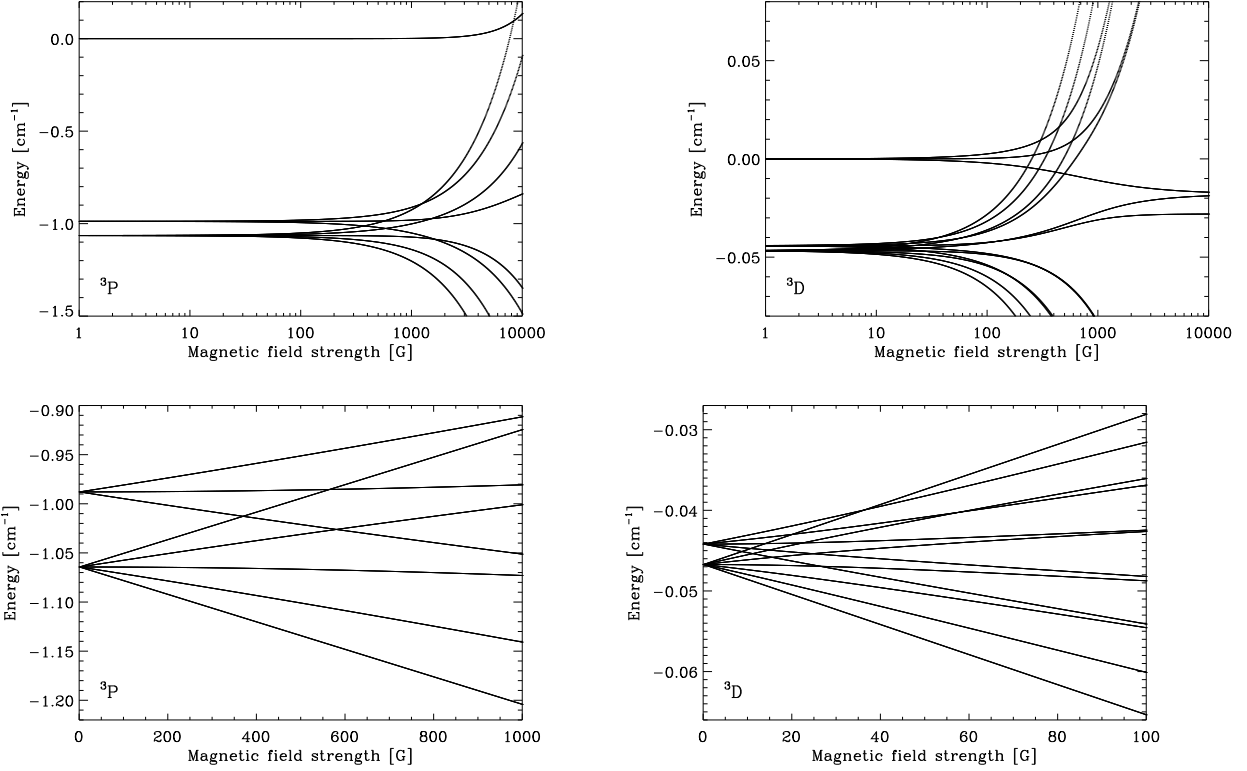


Fig. 3.— Energy splitting due to the presence of a magnetic field for the upper levels of the 10830 Å multiplet (left panels) and for the upper levels of the D_3 multiplet at 5876 Å (right panels). Note that the regimes where level crossings and repulsions occur are different for the two terms. They can be better identified in the lower panels. The energy of each level is referred to the energy of the level with the smallest value of J at zero magnetic field (i.e., $J = 0$ for the upper levels of the 10830 Å multiplet and $J = 1$ for the upper levels of the D_3 multiplet). The energy separation at $B = 0$ G is obtained from the information presented in Fig. 2.

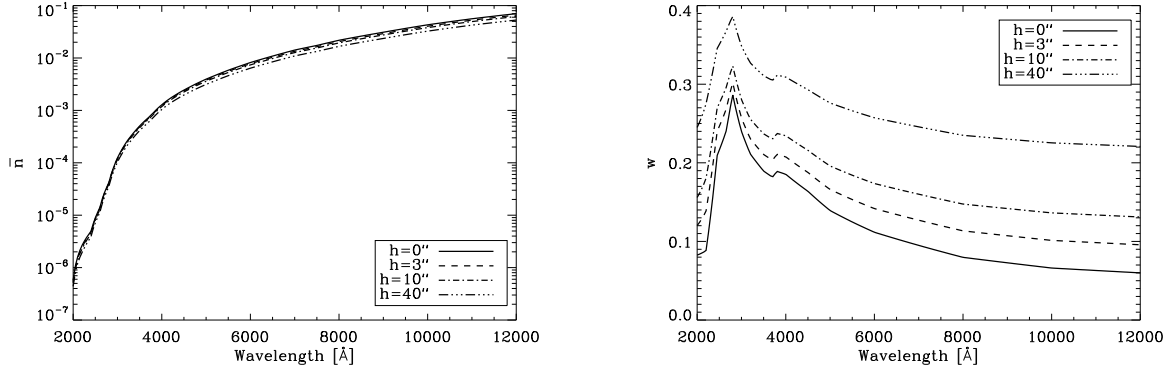


Fig. 4.— These two quantities (see Eqs. 19) characterize the radiation field that produces optical pumping processes in the He I atoms. The number of photons per mode \bar{n} (*left panel*) is proportional to the mean intensity, J_0^0 , while the anisotropy factor w (*right panel*) is proportional to the J_0^2 tensor of the radiation field. Both quantities have been obtained using the limb-darkening data tabulated by Pierce (2000). The figures show also the variation of these quantities with the atmospheric height at which the slab of helium atoms is assumed to be located. Note that, while the number of photons per mode is almost insensitive to h , the geometrical effects produce a significant variation on the anisotropy factor.

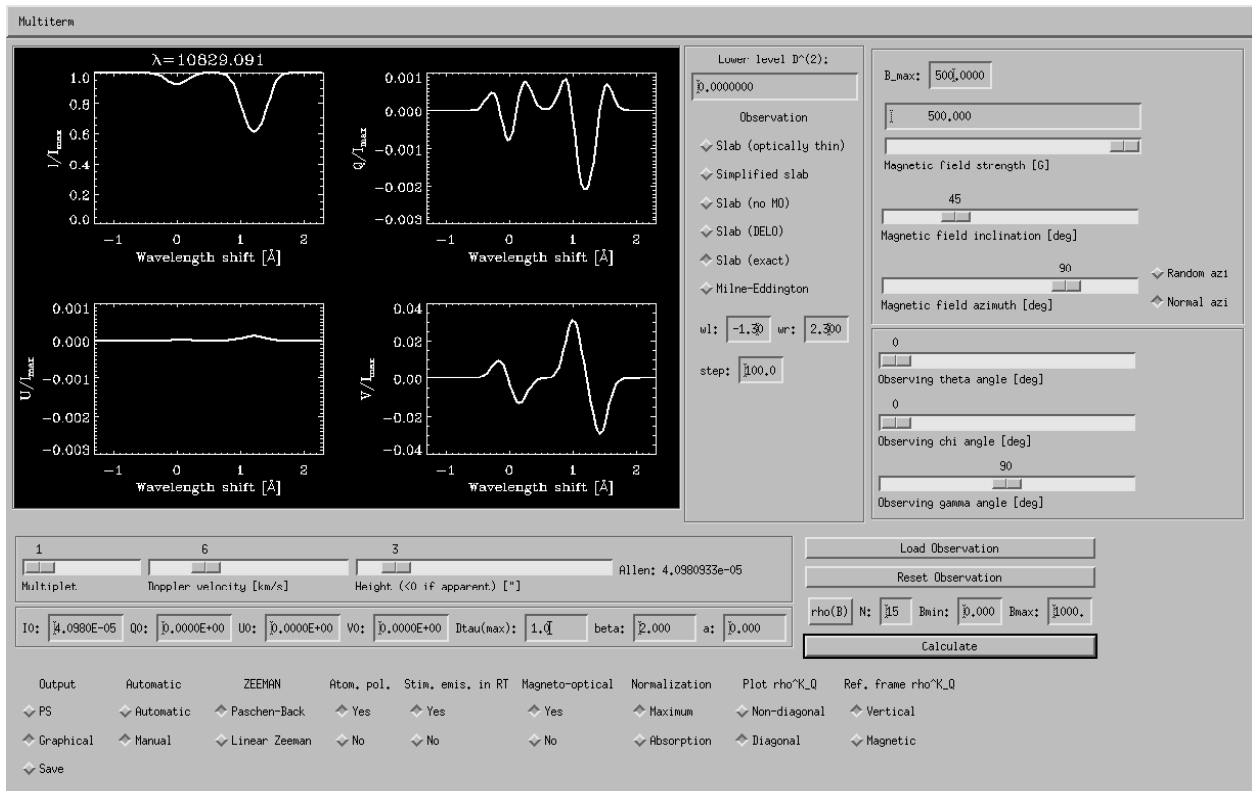


Fig. 5.— Screen dump of the graphical front-end used for the synthesis.

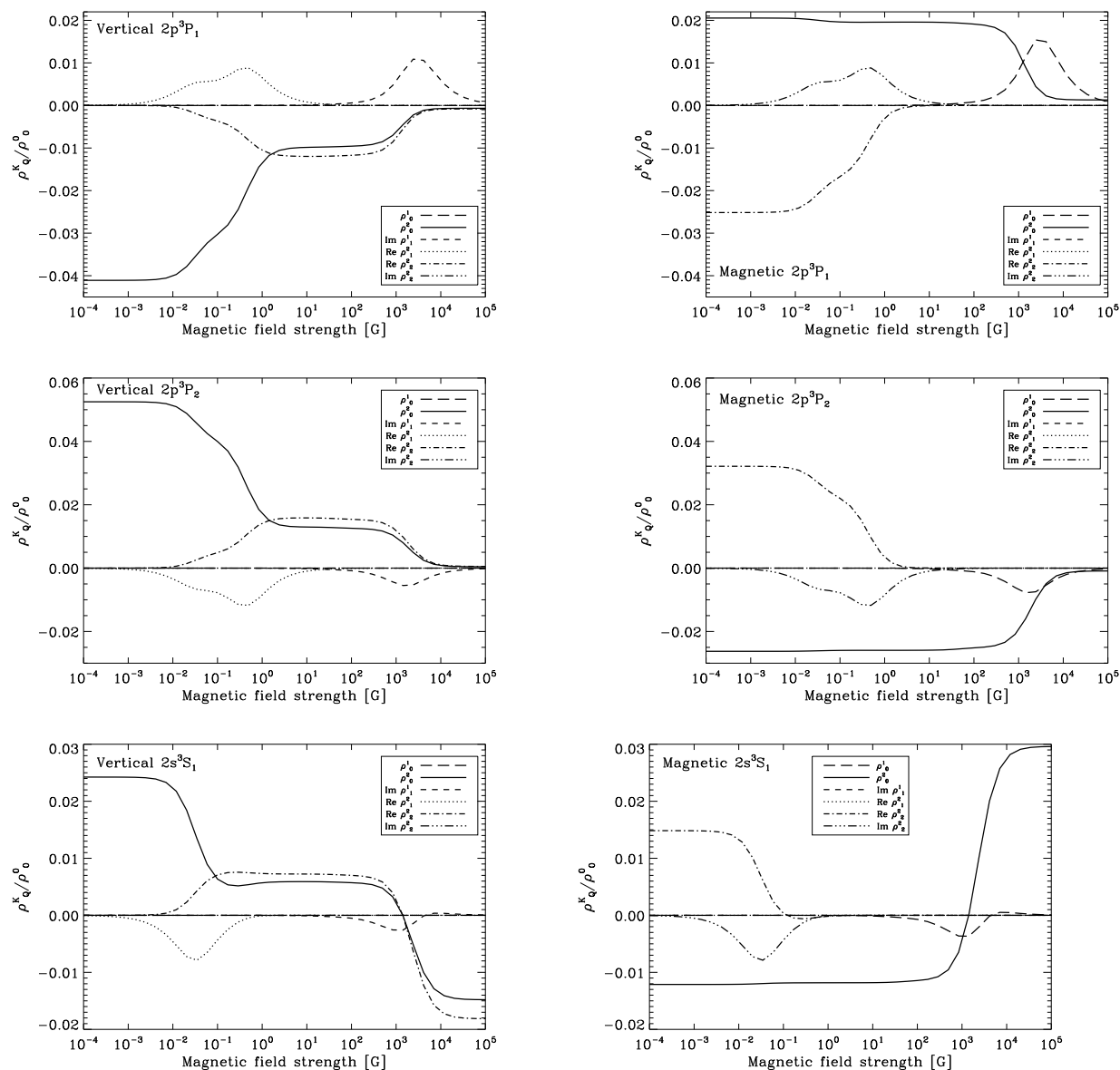


Fig. 6.— Variation of the fractional population imbalances, $\rho_0^K(J)/\rho_0^0(J)$, and of the non-zero quantum coherences between magnetic sublevels pertaining to a given J -level, $\rho_Q^K(J)/\rho_0^K(J)$, for different values of the strength of a horizontal magnetic field. We show these quantities for the $J_u = 1$ and $J_u = 2$ levels of the upper term of the 10830 Å transition (upper and middle panel, respectively) and for the $J_l = 1$ level of the lower term of the 10830 Å transition (lower panel). The left panels show the results for the “vertical” reference frame in which the quantization axis is chosen along the symmetry axis of the radiation field, while the right panels show the results for the magnetic field reference frame in which the quantization axis is chosen along the (horizontal) magnetic field vector. Note that, at $B \approx 0$ G, only population imbalances are present in the vertical reference frame, while both population imbalances and coherences are present in the magnetic reference frame. Note that in the magnetic field reference frame the quantum coherences are zero and $\rho_0^2(J)$ is constant for $10 < B < 100$ G.

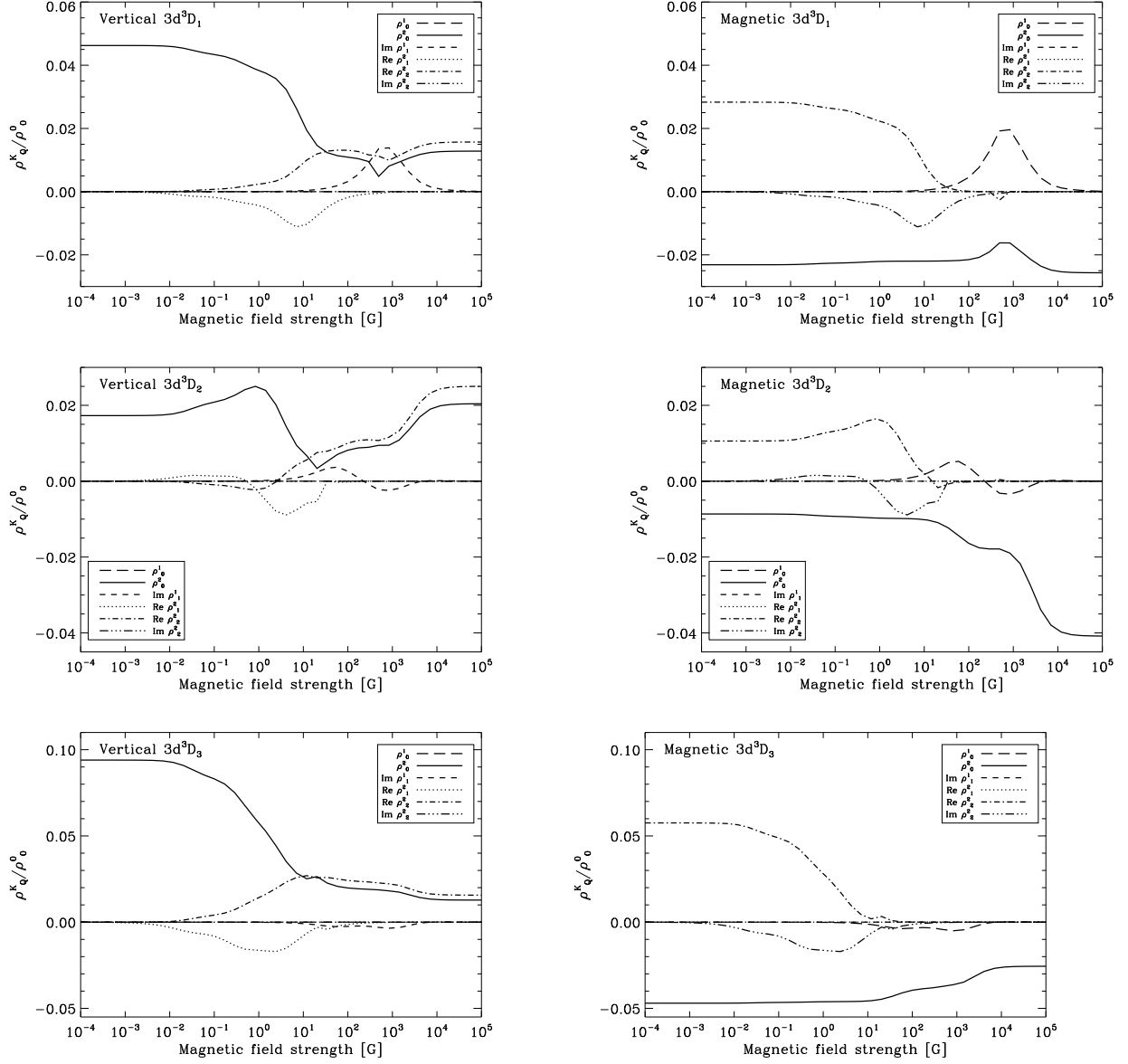


Fig. 7.— Same as Fig. 6, but for the J -levels of the upper term of the He I D_3 multiplet.

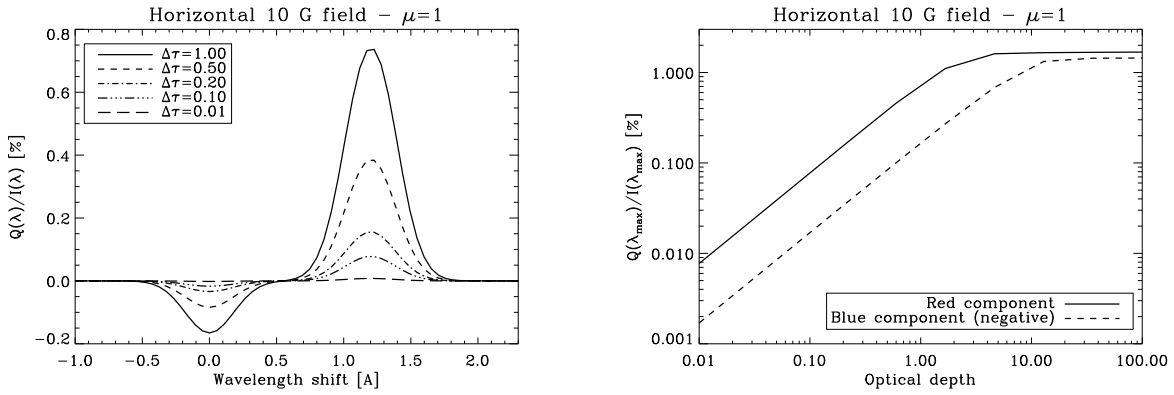


Fig. 8.— Emergent fractional linear polarization at the solar disk center in the lines of the He I 10830 Å multiplet, assuming that a constant-property slab of helium atoms at a height of 3 arcseconds is permeated by a horizontal magnetic field of 10 G. The various Q/I profiles of the left panel correspond to the slab’s optical thickness indicated in the inset, calculated at the wavelength of the red blended component. The right panel indicates that the fractional polarization amplitudes of the red and blue components increase exponentially with the slab’s optical thickness, till line saturation sets in. These calculations have been carried out using the exact solution of the radiative transfer equation given by Eq. (5). The positive reference direction for the definition of the Stokes Q parameter lies along the horizontal magnetic field vector.

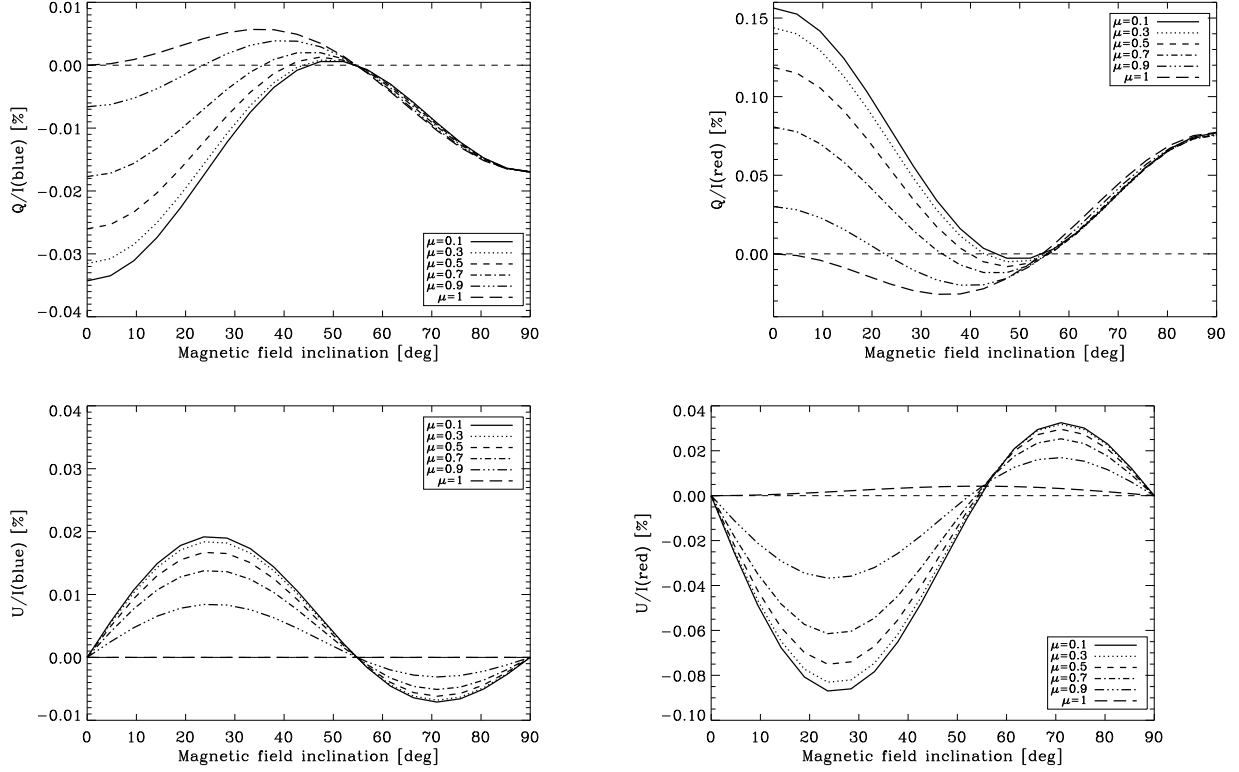


Fig. 9.— Variation of the linear polarization at the line center of the blue (left panel) and red (right panel) components of the He I 10830 Å multiplet for different inclinations of the magnetic field vector with respect to the local vertical and for different observing angles. The upper panels show Stokes Q while the lower panels show Stokes U , normalized to the value of Stokes I at the line center of each component. The calculations have been obtained assuming that a constant-property slab of helium atoms at a height of 3 arcseconds is permeated by a magnetic field of 10 G with an inclination θ_B with respect to the solar local vertical direction. The slab’s optical thickness at the wavelength of the red blended component is $\Delta\tau_{\text{red}} = 0.1$. The positive reference direction for Stokes Q is along the projection of the magnetic field vector on the solar surface, which makes an angle of 90° with any of the considered line-of-sights.

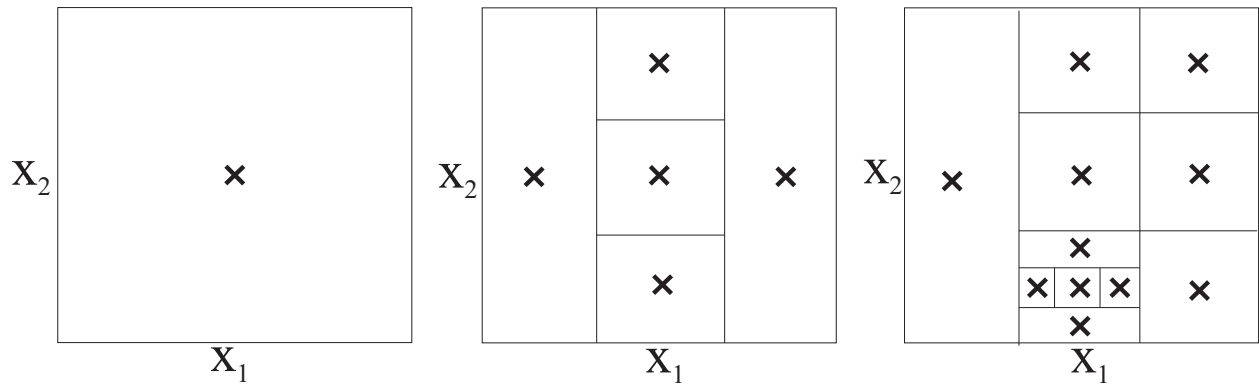


Fig. 10.— This figure illustrates the philosophy of the DIRECT method for searching the region where the global minimum is located. In this case, we present an illustrative example in two dimensions. After the evaluation of the merit function at some selected points inside each region, the DIRECT algorithm decides, using the Lipschitz condition, which rectangles should be further subdivided in case they are potentially optimal (optimal means that a low value of the merit function has been found or that the rectangles are large and a finer sampling has to be carried out). This method rapidly finds the region where the minimum is located.

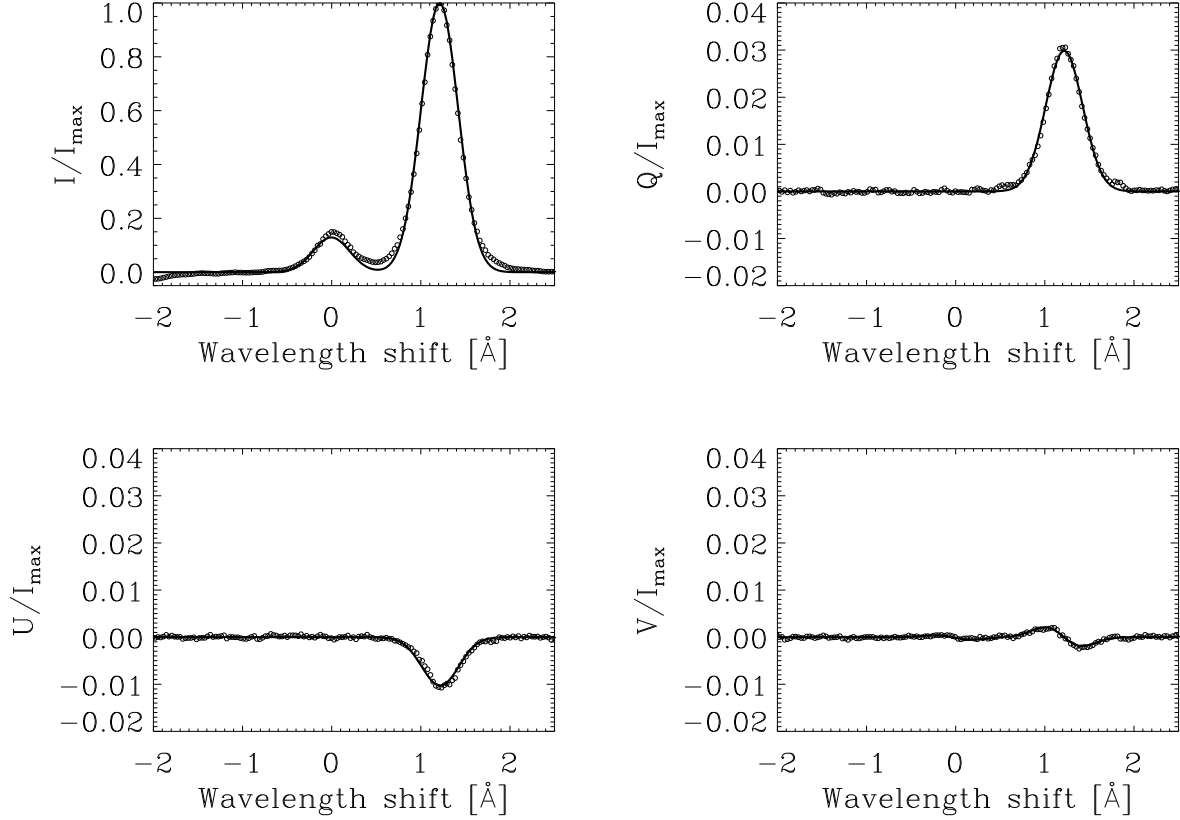


Fig. 11.— The solar prominence case. Example of the best theoretical fit obtained with the inversion code to some of the observed Stokes profiles presented in Merenda et al. (2006). The emergent Stokes profiles have been obtained by assuming an optically thin plasma. The inferred magnetic field vector is $B = 26.8$ G, $\theta_B = 25.5^\circ$ and $\chi_B = 161^\circ$ and the inferred thermal velocity $v_{\text{th}} = 7.97$ km s $^{-1}$. All these values are in good agreement with the results obtained by Merenda et al. (2006). The positive reference direction for Stokes Q is the parallel to the solar limb.

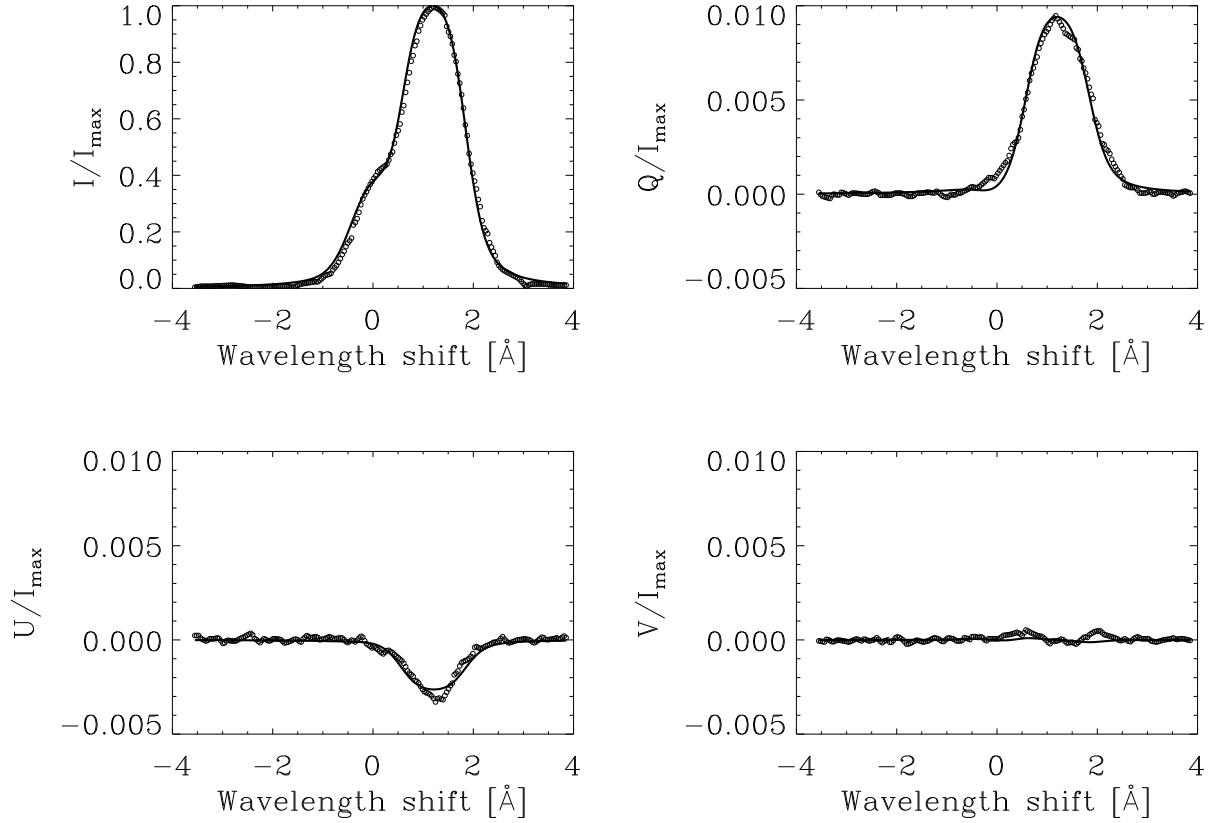


Fig. 12.— The case of solar chromospheric spicules. Example of the best theoretical fit obtained with the inversion code to the observed profiles presented in Trujillo Bueno et al. (2005). The emergent Stokes profiles have been obtained by taking into account radiative transfer effects in a constant-property slab model. The inferred magnetic field vector is $B = 2.6$ G, $\theta_B = 37^\circ$ and $\chi_B = 35^\circ$, although an equally good fit is obtained for other combinations like $B = 10$ G, $\theta_B = 37^\circ$ and $\chi_B = 172^\circ$ (see the text for more information). Furthermore, the inferred thermal velocity is $v_{\text{th}} = 13.9$ km s $^{-1}$, the slab’s optical thickness in the red blended component is $\Delta\tau_{\text{red}} = 2.54$ and the damping parameter is $a = 0.22$. The positive reference direction for Stokes Q is the parallel to the solar limb.

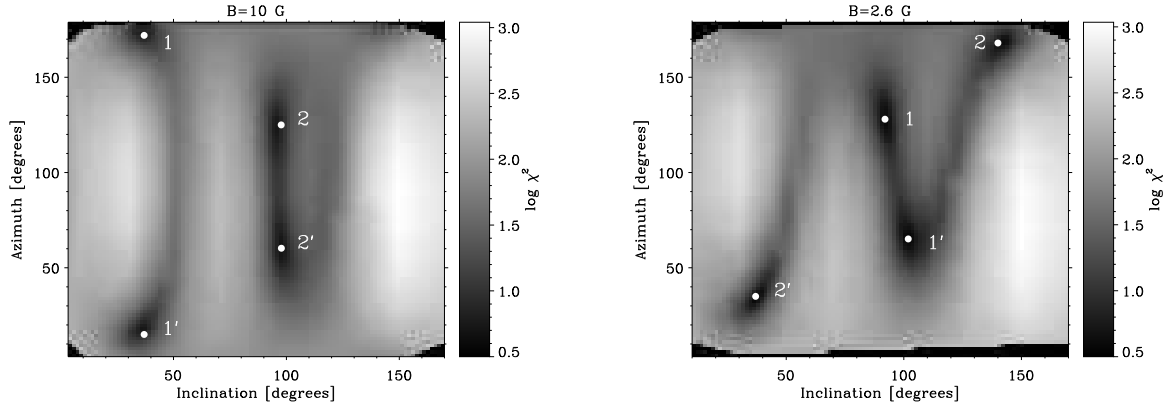


Fig. 13.— Values of the χ^2 -function for the possible fits of the Stokes profiles of the spicular material observed by Trujillo Bueno et al. (2005), after considering several combinations of the inclination and azimuth of the magnetic field vector. We fixed the thermal velocity, the optical depth of the slab and the damping constant to the following values: $v_{\text{th}} = 13.9 \text{ km s}^{-1}$, $\Delta\tau_{\text{red}} = 2.54$ and $a = 0.22$. The magnetic field strength is 10 G in the left panel while it is 2.6 G in the right panel. Note the presence of several local minima. The white dots indicate the position of the global minimum of the χ^2 -function. The solutions 1 and 2 correspond to the Van-Vleck ambiguity. The same happens for the solutions 1' and 2'. Additionally, the solutions 1 and 1' are equivalent for the code even if they do produce a sign change in the Stokes V signal because the observed Stokes V profile is at the level of noise. The same happens for the solutions 2 and 2'.

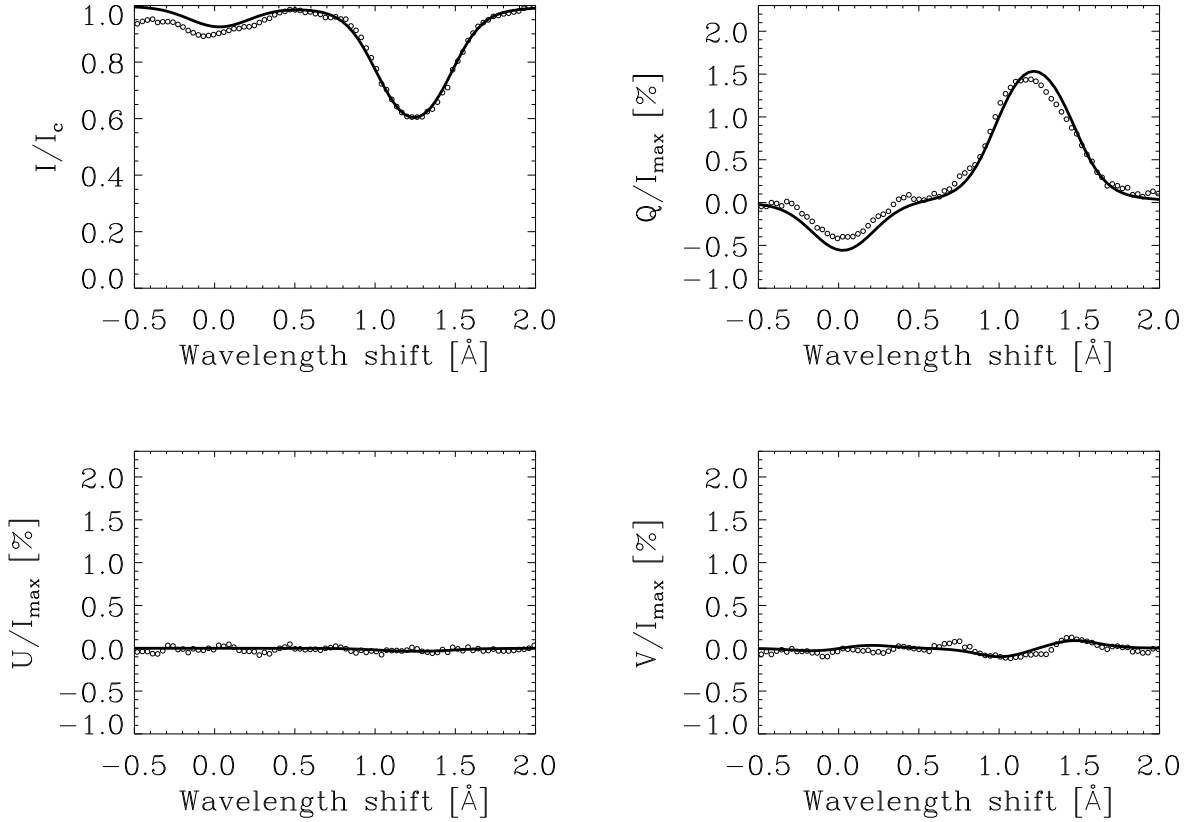


Fig. 14.— The case of a solar coronal filament. Example of the Stokes profiles of the He I 10830 Å multiplet observed in a coronal filament at solar disk center. Our results confirm the conclusions of Trujillo Bueno et al. (2002b), since we obtain $\Delta\tau = 0.86$, $v_{\text{th}} = 6.6$ km s^{-1} , $a = 0.19$, $B = 18$ G and $\theta_B = 105^\circ$. The positive direction of Stokes Q is parallel to the projection of the magnetic field vector on the solar surface.

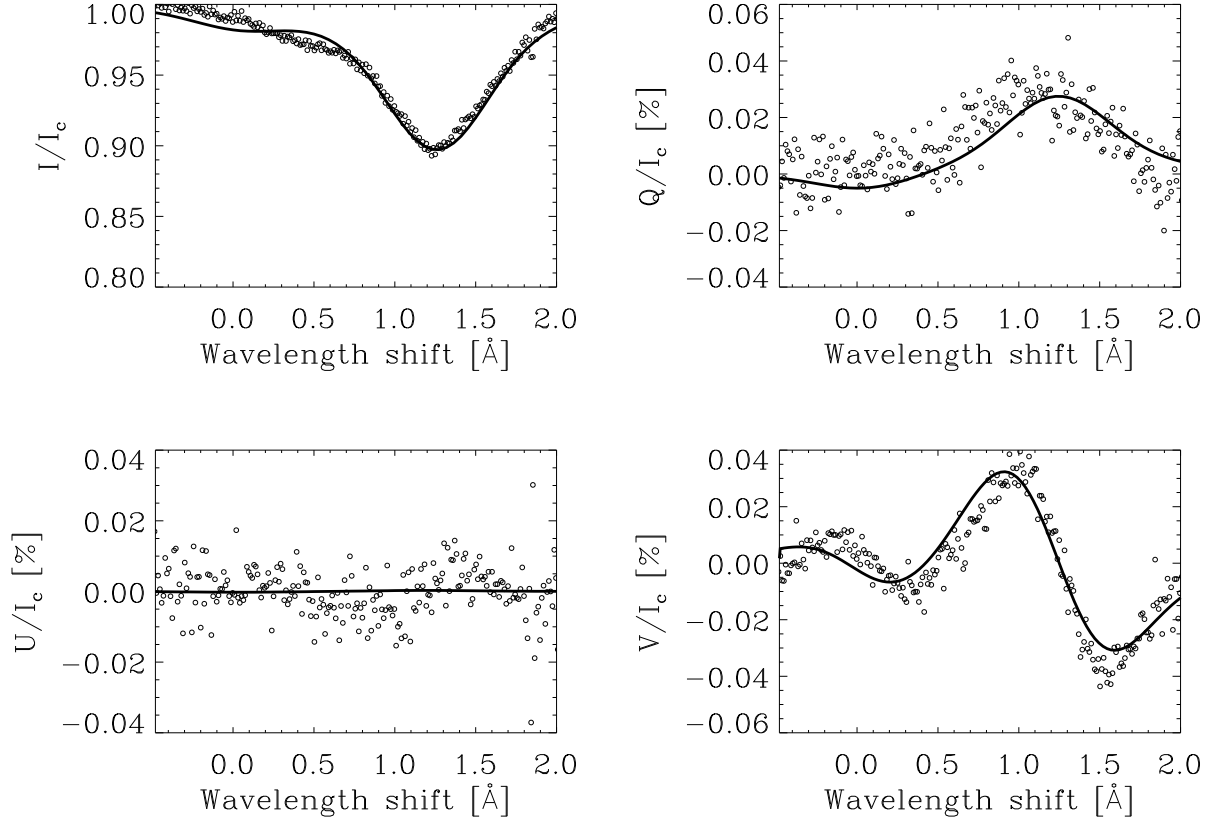


Fig. 15.— The quiet chromosphere case. Example of the Stokes profiles of the He I 10830 Å multiplet observed in a disk center ($\mu = 0.98$) internetwork region surrounded by an enhanced network region of almost circular shape. The observed Stokes profiles selected for the inversion correspond to a temporal and spatial average within the internetwork region. The solid line presents a fit to the observations which corresponds to a magnetic field vector with $B = 35$ G, $\theta_B = 21^\circ$ and $\chi_B = 0^\circ$. The inferred optical depth in the red blended component is $\Delta\tau_{\text{red}} \approx 0.2$, while $v_{\text{th}} = 9.2$ km s $^{-1}$ and $a = 0.62$. An equally good fit is obtained for other field configurations like $B = 47$ G, $\theta_B = 47^\circ$ and $\chi_B = 0^\circ$. The fact that with a $\theta_B < 54.74^\circ$ the Stokes Q signal of the red component is positive (after our rotation of the reference system to minimize Stokes U) indicates that the reference direction for Stokes Q lies along the direction perpendicular to the projection of the magnetic field vector on the solar disk (see the $\mu = 1$ case of Fig. 9).

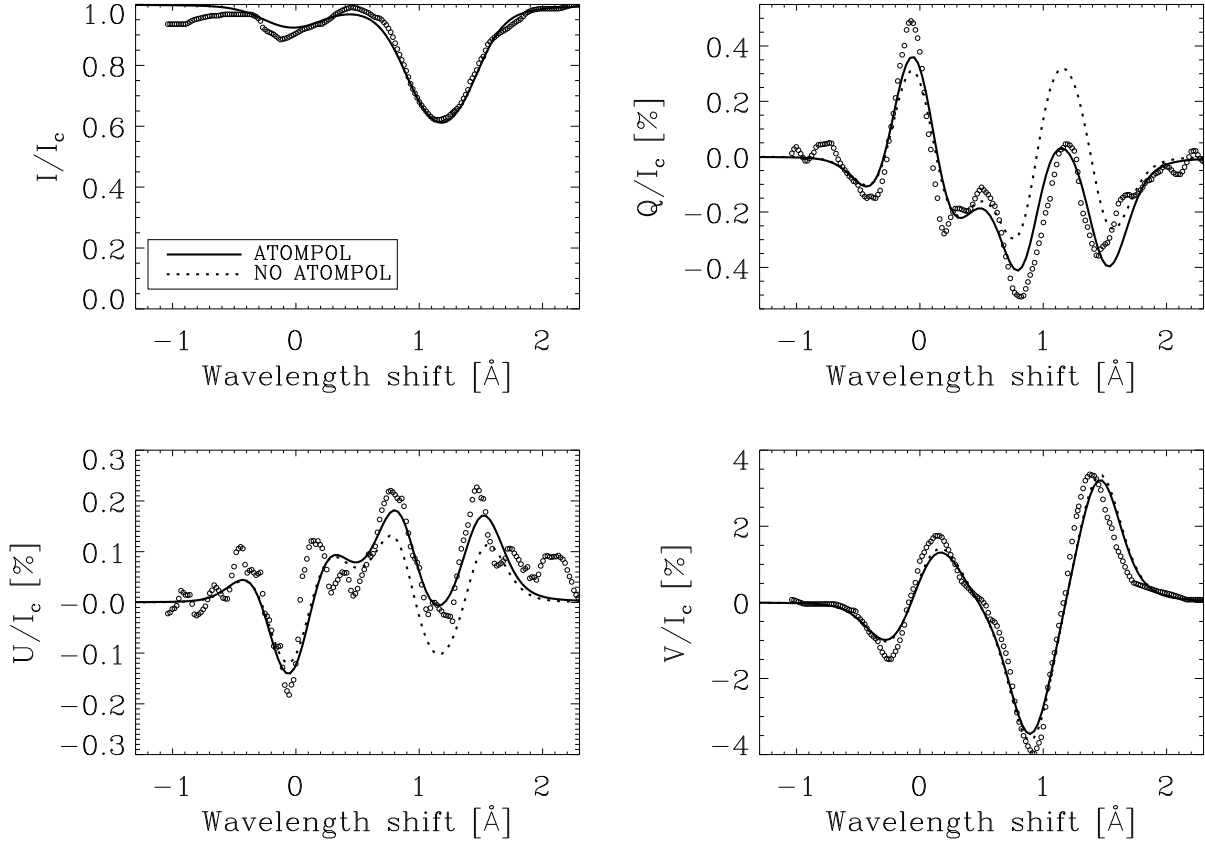


Fig. 16.— The case of an emerging flux region. Example of the Stokes profiles of the He I 10830 Å multiplet in an emerging flux region located at $\mu = 0.8$. The circles present the observed Stokes profiles obtained from Fig. 2 of Lagg et al. (2004), but after rotating the reference system by -56° to have the reference direction for the Stokes Q profile along the direction perpendicular to the straight line joining the disk center with the observed region. For this reason the inversion has been carried out using $\chi = 0^\circ$ and $\gamma = 90^\circ$ (see Fig. 1). The solid line presents the best fit obtained with our inversion code, taking into account the effect of atomic polarization on the emergent Stokes profiles, in addition to the Zeeman effect treated within the framework of the Paschen-Back effect theory. This full solution corresponds to a magnetic field vector with $B = 1073$ G, $\theta_B = 86^\circ$ and $\chi_B = 170.7^\circ$, while $\Delta\tau_{\text{red}} = 1.07$, $v_{\text{th}} = 7.24$ km s $^{-1}$ and $a = 0.25$. The dotted line is the best fit obtained when neglecting atomic polarization. These results confirm the conclusion by Trujillo Bueno & Asensio Ramos (2007) that the presence of atomic polarization in the levels of the He I 10830 Å multiplet produces observable signatures on the emergent Stokes profiles even for fields as large as 1000 G. We point out that there is a typing error in the caption of figure 3 of Trujillo Bueno & Asensio Ramos (2007), since the theoretical Stokes profiles in that figure were obtained for a LOS with $\mu = \cos\theta = 0.8$ (i.e., not for the $\mu = 1$ forward scattering case) and with $\chi = \gamma = 0^\circ$ (see Fig. 1).

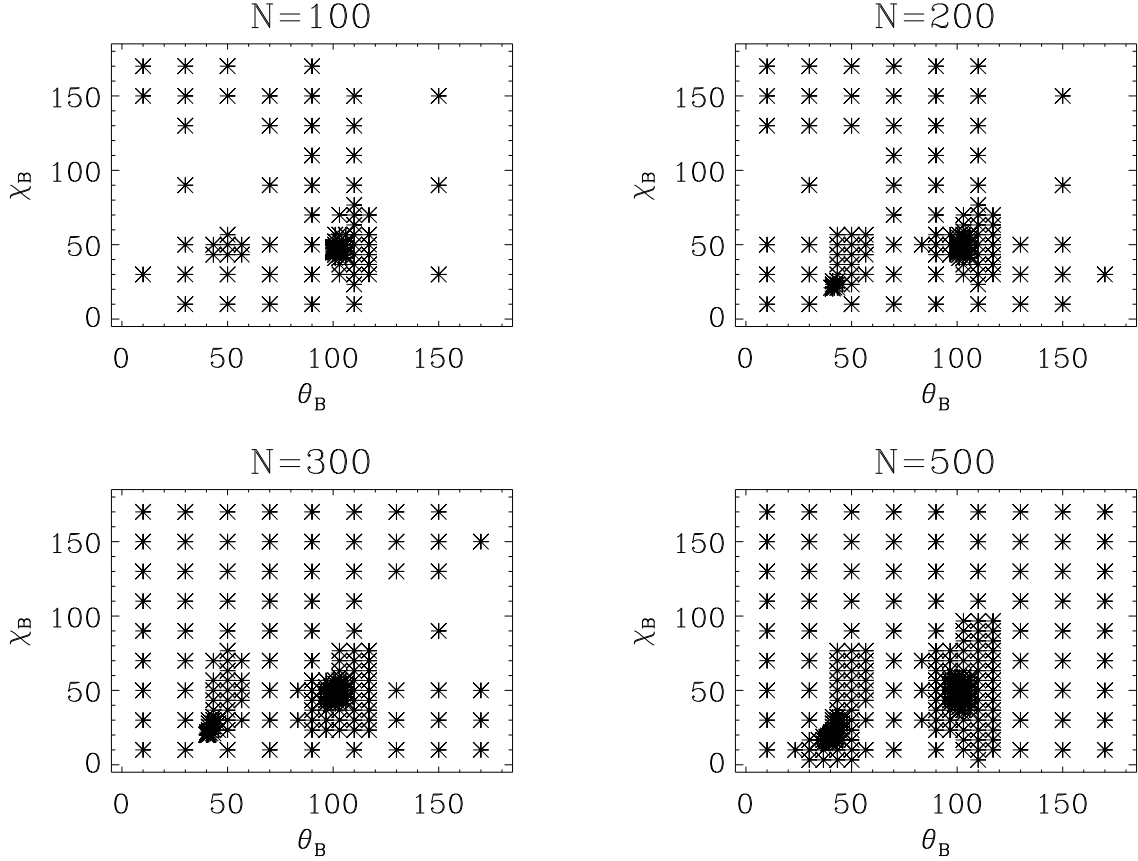


Fig. 17.— Value of θ_B and χ_B at which the merit function is evaluated for detecting possible ambiguities using the DIRECT method. The number N of function evaluations is shown on the top of each panel. The two global minima seen in the figures result from the Van Vleck ambiguity, showing two different magnetic field vectors that produce the same emergent Stokes profiles. This figure illustrates the power of the DIRECT method, which allows to recover the two values of the magnetic field vector in this ambiguous case with less than 200 function evaluations. We have shown only half of the space of parameters in order to avoid the 180° ambiguity.

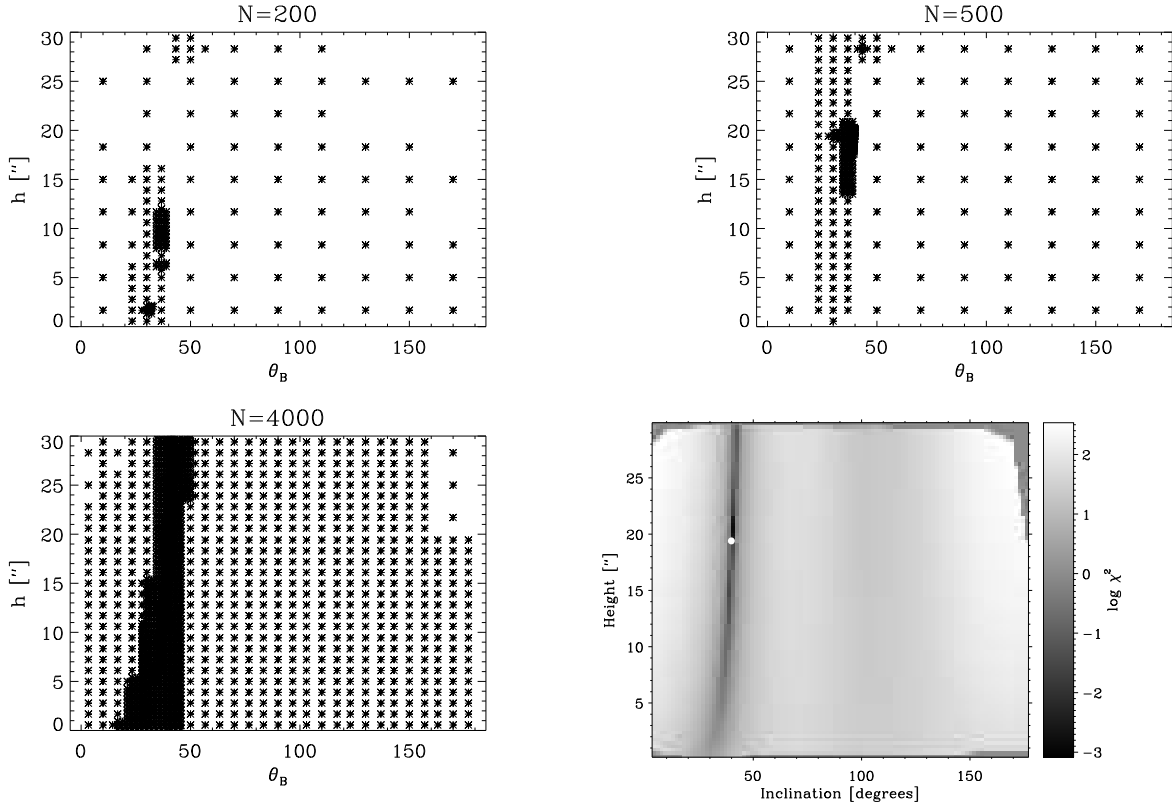


Fig. 18.— Value of θ_B and h at which the merit function is evaluated when using the DIRECT method for the inversion of the off-limb Stokes profiles indicated in the text (upper panels and bottom left panel). The number N of function evaluations is shown on the top of each panel. The presence of a very deep and shallow strip where the minimum is located makes it difficult to obtain it. The DIRECT method needs at least 1000 function evaluations to find the region where the minimum is located. The bottom right panel shows the value of the χ^2 merit function with the white dot indicating the combination of parameters that give the smallest value of the merit function. This is an example of a problem that poses severe difficulties to any gradient-based method like Levenberg-Marquardt.

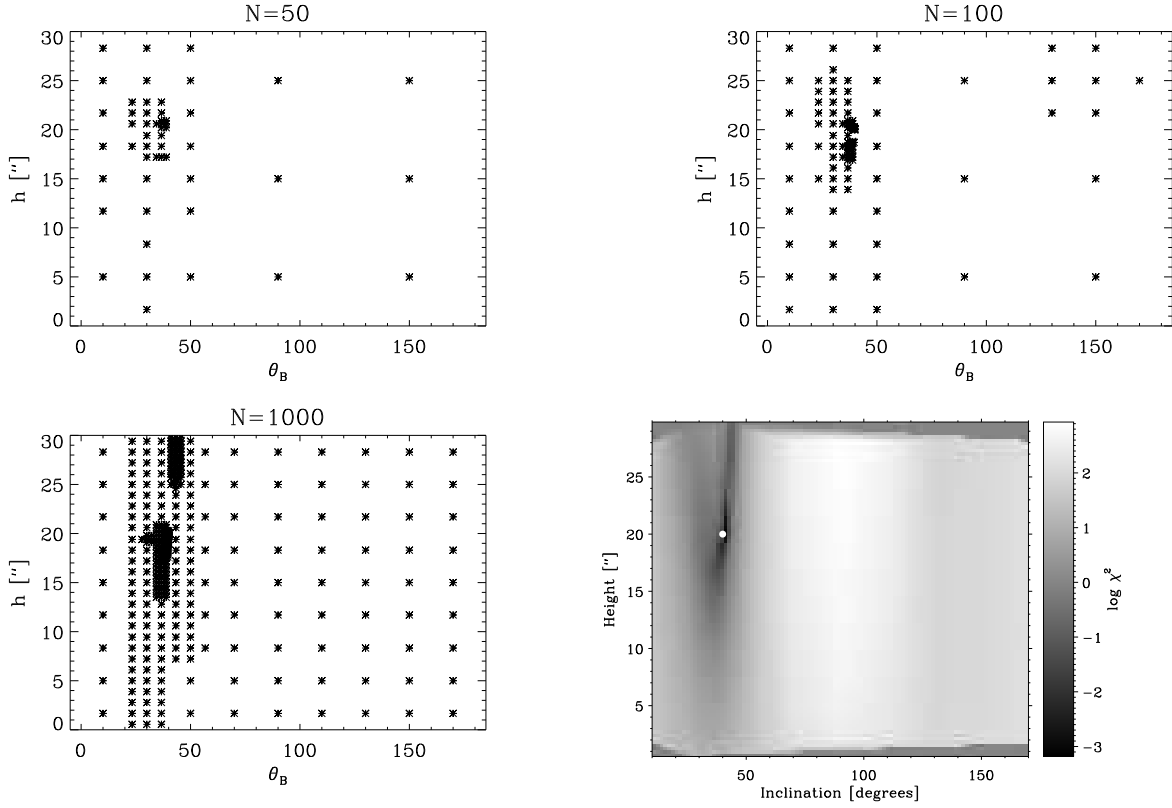


Fig. 19.— Value of θ_B and h at which the merit function is evaluated when using the DIRECT method for the inversion of the on-disk Stokes profiles indicated in the text. The number N of function evaluations is shown on the top of each panel (upper panels and bottom left panel). Even with only $N = 50$, the DIRECT method is able to locate the region of the global minimum. When the number of evaluations increases, it converges towards the values $\theta_B = 40^\circ$ and $h = 20''$. The bottom right panel shows the value of the χ^2 merit function with the white dot indicating the combination of parameters that give the smallest value of the merit function.

Table 1: Parameters of the inversion.

Free parameter	Description	Units
B	Magnetic field strength	gauss
θ_B	Inclination of the magnetic field vector with respect to the vertical	degrees
χ_B	Azimuth of the magnetic field vector	degrees
v_{th}	Thermal velocity affecting the width of the line	km s^{-1}
v_{mac}	Bulk velocity of the plasma leading to a red/blue-shift	km s^{-1}
$\Delta\tau$	Optical depth of the line	–
a	Line damping parameter	–

Table 2: Inversion scheme.

Step	Method	Free parameters	Stokes profiles
1	DIRECT	$v_{\text{th}}, v_{\text{mac}}, \Delta\tau, a$	I
2	LM	$v_{\text{th}}, v_{\text{mac}}, \Delta\tau, a$	I
3	DIRECT	B, θ_B, χ_B	I, Q, U, V
4	LM	B, θ_B, χ_B	I, Q, U, V

REFERENCES

- Andretta, V., & Jones, H. P. 1997, *ApJ*, 489, 375
- Asensio Ramos, A., Martínez González, M. J., & Rubiño Martín, J. A. 2007, *A&A*, 476, 959
- Avrett, E. H., Fontenla, J. M., & Loeser, R. 1994, Formation of the solar 10830 Å line (Infrared Solar Physics, IAU Symp. No. 154, eds. D.M. Rabin, J.T. Jefferies, and C. Lindsey, Kluwer, Dordrecht, pp. 35-47), 35
- Bartholomew-Biggs, M., Parkhurst, S., & Wilson, S. 2002, *Comp. Optim. Appl.*, 21, 311
- Belluzzi, L., Trujillo Bueno, J., & Landi Degl’Innocenti, E. 2007, *ApJ*, 666, 588
- Bommier, V. 1980, *A&A*, 87, 109
- Bommier, V., Landi Degl’Innocenti, E., Leroy, J.-L., & Sahal-Brechot, S. 1994, *Sol. Phys.*, 154, 231
- Casini, R., & Judge, P. G. 1999, *ApJ*, 522, 524
- Casini, R., & Manso Sainz, R. 2005, *ApJ*, 624, 1025
- Casini, R., Bevilacqua, R., & López Ariste, A. 2005, *ApJ*, 622, 1265
- Casini, R., López Ariste, A., Tomczyk, S., & Lites, B. W. 2003, *ApJ*, 598, L67
- Centeno, R., Collados, M., & Trujillo Bueno, J. 2006, *ApJ*, 640, 1153
- Centeno, R., Trujillo Bueno, J., Uitenbroek, H., & Collados, M. 2008, *ApJ*, 677, 742
- Collados, M., Lagg, A., Díaz García, J. J., Hernández Suárez, E., López López, R., Páez Mañá, E., & Solanki, S. K. 2007, in *Astronomical Society of the Pacific Conference Series*, Vol. 368, *The Physics of Chromospheric Plasmas*, ed. P. Heinzel, I. Dorotovič, & R. J. Rutten, 611
- Condon, E. U., & Shortley, G. H. 1935, *The Theory of Atomic Spectra* (Cambridge: Cambridge University Press)
- Cox, S., Haftka, R., Baker, C., Grossman, B., Mason, W., & Watson, L. 2001, *J. Global Optim.*, 21, 415
- Drake, G. W. F., & Martin, W. C. 1998, *Can. J. Phys.*, 76, 679

- Edmonds, A. R. 1960, *Angular Momentum in Quantum Mechanics* (Princeton University Press)
- Gutowsky, M. W. 2004, in VII Domestic Conference on Evolutionary Algorithms and Global Optimization, cs.NE/0512019
- Harvey, J., & Hall, D. 1971, in IAU Symp. 43: Solar Magnetic Fields, ed. R. Howard, 279
- Horst, R., & Pardalos, P. M. 1995, *Handbook of Global Optimization* (Dordrecht: Kluwer Academic Publishers)
- House, L. L. 1977, *ApJ*, 214, 632
- Jones, D. R., Perttunen, C. D., & Stuckmann, B. E. 1993, *Journal of Optimization Theory and Applications*, 79, 157
- Lagg, A. 2007, *Advances in Space Research* 39, 1734
- Lagg, A., Woch, J., Krupp, N., & Solanki, S. K. 2004, *A&A*, 414, 1109
- Landi Degl’Innocenti, E. 1982, *Sol. Phys.*, 79, 291
- Landi Degl’Innocenti, E., Landi Degl’Innocenti, M. 1985, *Sol. Phys.*, 97, 239
- Landi degl’Innocenti, E., & Bommier, V. 1993, *ApJ*, 411, L49
- Landi Degl’Innocenti, E., & Landolfi, M. 2004, *Polarization in Spectral Lines* (Kluwer Academic Publishers)
- Lin, H., Penn, M. J., & Kuhn, J. R. 1998, *ApJ*, 493, 978
- Ljungberg, L., Holmgren, S., & Carlborg, Ö. 2004, *Bioinformatics*, 20, 1887
- López Ariste, A., & Casini, R. 2002, *ApJ*, 575, 529
- . 2005, *A&A*, 436, 325
- MacKay, D. J. C. 2003, *Information Theory, Inference, and Learning Algorithms* (Cambridge University Press)
- Manso Sainz, R., & Trujillo Bueno, J. 2003a, in ASP Conf. Ser. 307: Solar Polarization 3, ed. J. Trujillo Bueno & J. Sánchez Almeida, 251
- Manso Sainz, R., & Trujillo Bueno, J. 2003b, *Phys. Rev. Lett.*, 91, 111102

- Martínez Pillet, V., Collados, M., Bellot Rubio, L. R., Rodríguez Hidalgo, I., Ruiz Cobo, B., & Soltau, D. 1999, in *Astronomische Gesellschaft Meeting Abstracts*, vol. 15
- Merenda, L., Trujillo Bueno, J., Landi Degl’Innocenti, E., & Collados, M. 2006, *ApJ*, 642, 554
- Pierce, K. 2000, in *Allen’s Astrophysical Quantities*, ed. A. N. Cox (New York: Springer Verlag and AIP Press)
- Press, W. H., Teukolsky, S. A., Vetterling, W. T., & Flannery, B. P. 1986, *Numerical Recipes* (Cambridge: Cambridge University Press)
- Querfeld, C. W., Smartt, R. N., Bommier, V., Landi Degl’Innocenti, E., House, L. L. 1985, *Sol. Phys.*, 96, 277
- Ramelli, R., Bianda, M., Merenda, L., & Trujillo Bueno, J. 2006a, in *ASP Conf. Ser.*, Vol. 358, *Solar Polarization 4*, ed. R. Casini & B. W. Lites, 448
- Ramelli, R., Bianda, M., Trujillo Bueno, J., Merenda, L., & Stenflo, J. O. 2006b, in *ASP Conf. Ser.*, Vol. 358, *Solar Polarization 4*, ed. R. Casini & B. W. Lites, 471
- Rees, D. E., Murphy, G. A. & Durrant, C. J. 1989, *ApJ*, 339, 1093
- Rüedi, I., Keller, C. U., & Solanki, S. K. 1996, *Sol. Phys.*, 164, 265
- Socas-Navarro, H., & Elmore, D. 2005, *ApJ*, 619, L195
- Socas-Navarro, H., Trujillo Bueno, J., & Landi Degl’Innocenti, E. 2004, *ApJ*, 612, 1175
- Trujillo Bueno, J. 2001, in *ASP Conf. Ser. 236: Advanced Solar Polarimetry – Theory, Observation, and Instrumentation*, ed. M. Sigwarth, 161
- Trujillo Bueno, J. 2003, in *Stellar Atmosphere Modeling*, ed. I. Hubeny, D. Mihalas, & K. Werner, *ASP Conf. Ser. 288* (San Francisco: ASP), 551
- Trujillo Bueno, J. 2005, in *ESA SP-600: The Dynamic Sun: Challenges for Theory and Observations*, ed. D. Danesy, S. Poedts, A. De Groof, & J. Andries, 7
- Trujillo Bueno, J., & Asensio Ramos, A. 2007, *ApJ*, 655, 642
- Trujillo Bueno, J., & Shchukina, N. 2007, *ApJ*, 664, L135
- Trujillo Bueno, J., Casini, R., Landolfi, M., & Landi Degl’Innocenti, E. 2002a, *ApJ*, 566, L53

Trujillo Bueno, J., Landi Degl’Innocenti, E., Collados, M., Merenda, L., & Manso Sainz, R. 2002b, *Nature*, 415, 403

Trujillo Bueno, J., Merenda, L., Centeno, R., Collados, M., & Landi Degl’Innocenti, E. 2005, *ApJ*, 619, L191

Wiese, W. L., Smith, M. W., & Glennon, B. M. 1966, *Natl. Stand. Ref. Data Ser.*, Vol. I (Natl Bur. Stand. (U.S.), NSRDS-NBS 4)

Table 3: He I atomic data.

Transition ($u \rightarrow \ell$)	Air wavelength [\AA]	$A(\beta_u L_u S J_u \rightarrow \beta_\ell L_\ell S J_\ell)$ [s^{-1}]	$B_{\text{critical}}^{\text{upper}}$ [G]
2p $^3\text{P}_0 - 2\text{s } ^3\text{S}_1$	10829.0911	1.022×10^7	undefined
2p $^3\text{P}_1 - 2\text{s } ^3\text{S}_1$	10830.2501	1.022×10^7	0.77
2p $^3\text{P}_2 - 2\text{s } ^3\text{S}_1$	10830.3398	1.022×10^7	0.77
3p $^3\text{P}_0 - 2\text{s } ^3\text{S}_1$	3888.6046	9.478×10^6	undefined
3p $^3\text{P}_1 - 2\text{s } ^3\text{S}_1$	3888.6456	9.478×10^6	0.72
3p $^3\text{P}_2 - 2\text{s } ^3\text{S}_1$	3888.6489	9.478×10^6	0.72
3s $^3\text{S}_1 - 2\text{p } ^3\text{P}_0$	7065.7085	3.080×10^6	0.18
3s $^3\text{S}_1 - 2\text{p } ^3\text{P}_1$	7065.2150	9.250×10^6	0.53
3s $^3\text{S}_1 - 2\text{p } ^3\text{P}_2$	7065.1769	1.540×10^7	0.88
3d $^3\text{D}_1 - 2\text{p } ^3\text{P}_0$	5875.9663	3.920×10^7	8.92
3d $^3\text{D}_2 - 2\text{p } ^3\text{P}_1$	5875.6405	5.290×10^7	5.16
3d $^3\text{D}_1 - 2\text{p } ^3\text{P}_1$	5875.6251	2.940×10^7	6.69
3d $^3\text{D}_3 - 2\text{p } ^3\text{P}_2$	5875.6150	7.060×10^7	6.02
3d $^3\text{D}_2 - 2\text{p } ^3\text{P}_2$	5875.6141	1.760×10^7	1.72
3d $^3\text{D}_1 - 2\text{p } ^3\text{P}_2$	5875.5987	1.960×10^6	0.45